Bollettino di Geofisica Teorica ed Applicata Vol. 61, n. 4, pp. 555-588; December 2020
DOI 10.4430/bgta0324

A fractal-based outranking approach for integrating geochemical, geological, and geophysical data

H. Ghaeminejad[1], M. Abedi[1], P. Afzal[2], F. Zaynali[1] and M. Yousefi[3]

[1] *School of Mining Engineering, College of Engineering, University of Tehran, Iran*
[2] *Department of Petroleum and Mining Engineering, South Tehran Branch, Islamic Azad University, Tehran, Iran*
[3] *Faculty of Engineering, Malayer University, Malayer, Iran*

(Received: 26 October 2019; accepted: 29 February 2020)

ABSTRACT This study presents an adaption of outranking techniques, incorporating fractal concepts for mineral prospectivity analysis, in complex geological settings with complicated mineral systems. This study shows that knowledge deficiency in understanding complex mineralisation systems can be redressed by fractal modelling in terms of exploration evidence data classification. Then, the outranking approaches are used to integrate indicator layers derived via multi-disciplinary geospatial data sets for the generation of reliable exploration targets and prospects. To illustrate how the proposed method works and to demonstrate its effectiveness in generating reliable exploration targets, we used a data set for gold mineralisation prospects in the Alut region, NW Iran. There are geochemical, geological, structural, remote sensing, and geophysical layers used for this purpose. Fractal modelling is utilised for classification of different layers and final map.

Key words: exploratory data set, fractal model, outranking approaches, mineral prospectivity mapping, Alut, Iran.

1. Introduction

Prospectivity analysis dealing with the generation of mineral exploration targets has been at the centre of attention over the past two decades owing to its ability to delimit areas regarding their mineral endowments, so that decision making in the way of further exploration is facilitated (Bonham-Carter, 1989, 1994; Harris *et al*., 2003; Porwal *et al*., 2006; Nykänen, 2008; Carranza, 2009; Zuo and Carranza, 2011; Abedi and Norouzi, 2012, 2016; Abedi *et al*., 2012a, 2012b, 2012c; Rezaei *et al*., 2015; Yousefi and Carranza, 2015a, 2015b, 2015c). In the procedure of prospectivity analysis, various exploratory geospatial data sets are taken into consideration aiming at using the ability of different exploration techniques in prospecting undiscovered mineral deposits. Data integration means integrating multiple evidence layers to delineate potential areas in order to assist decision making (Yousefi and Carranza, 2015c). Thus, Mineral Prospectivity Mapping (MPM) is also known as a Multi-Criteria Decision Making (MCDM) technique (Yousefi and Carranza, 2015c; Panahi *et al*., 2017).

As pointed out by researchers, the main problem arising from MPM is the quantification of

spatial and genetic relationships between exploration evidence data and the targeted deposit-type sought (e.g. McCuaig and Hronsky, 2000, 2014; Almasi *et al*., 2017; Shahsavar *et al*., 2019), which must be contemplated before integration stage. The quantification is also referred to "weighting" of exploration data (e.g. Carranza *et al*., 1999; Carranza, 2009; Hosseini and Abedi, 2015). Weighting challenges are mainly due to our incomplete knowledge on ore-forming factors, i.e. the operation of a variety of complex geological processes (cf. McCuaig and Hronsky, 2000, 2014; Yousefi and Carranza, 2015a), which may act diversely in different geological settings. Furthermore, the incomplete knowledge results in various kinds of uncertainty affecting our understanding of the geological processes and their translation into weighted evidence layers (e.g. Almasi *et al*., 2017). In this regard, attempting to develop a better method to redress modulating the above-mentioned weighting problems results in various MPM approaches, which could be categorised into five general groups, namely: data-driven, knowledge-driven, hybrid methods, weighting using subjectively-defined functions, and logistic-based approaches (e.g. Agterberg *et al*., 1990; Bonham-Carter, 1994; Agterberg and Bonham-Carter, 1999; Carranza and Hale, 2001, 2002a, 2002b, 2002c, 2003; Harris *et al*., 2003; Carranza *et al*., 2005, 2008a, 2008b; Porwal *et al*., 2006; Nykänen, 2008; Carranza, 2009; Zuo and Carranza, 2011; Abedi *et al*., 2012a, 2012b, 2012c, 2013a, 2013b, 2013c, 2015, 2016; Eberle and Paasche, 2012; Carranza and Laborte, 2015a, 2015b, 2016, 2017; Yousefi and Carranza, 2016, 2017; Yousefi and Nykänen, 2016, 2017).

Among the various MPM techniques, outranking approaches have been developed for making optimised decisions in MCDM problems. The concept of an outranking relation was extensively investigated and proposed by Roy (1974). Outranking techniques work based on two major steps (Bufardi *et al*., 2008): 1) construction of the outranking relations such as concordance and discordance indices with respect to each criterion, and 2) aggregation of the single outranking relations into a global outranking relation. Outranking approaches have been adapted for MPM and were successfully examined to delineate mineral exploration targets (e.g. Abedi, 2015; Abedi *et al*., 2015; Shahsavar *et al*., 2019).

This paper aims to adapt outranking approaches (Abedi and Norouzi, 2016; Abedi *et al*., 2016; Panahi *et al*., 2017), in conjunction with fractal concepts, in order to model mineral prospectivity in complex geological settings with complicated mineral systems (Nazarpour, 2018; Ahmadfaraj *et al*., 2019; Zadmehr and Shahrokhi, 2019). To achieve this and demonstrate how the method proposed can model mixed-mineralisation systems, we used a data set of gold mineralisation at a district-scale study in the Alut area, NW Iran, as an example. Subsequently, the VIKOR (Opricovic, 1998) and TOPSIS (Hwang and Yoon, 1981) methods, respectively involving two and three variants as the conventional and adjusted ones (Abedi and Norouzi, 2016; Abedi *et al*., 2016), were employed on evidence layers of fractal-based categorised spatial exploration data (Appendices A1 and A2). We applied a conventional multi-class index overlay MPM method (Bonham-Carter, 1994; Carranza, 2009) for comparison purposes as well.

2. Methodologies

In the first phase, different indicator criteria (i.e. geology, geophysics, geochemistry and remote sensing) were extracted from the geospatial data sets (Fig. 1, phase I), while their importance was taken into account by assigning appropriate weights through the Delphi method. The

Concentration-Number (C-N) multifractal model was used to categorise each layer by allocating new scores to each category (Mandelbrot, 1983; Hassanpour and Afzal, 2013). Then, outranking methods integrated such fractal-based layers as input features to generate the MPM. Highly favorable Au-bearing zones were extracted by using the Concentration-Area (C-A) fractal method (Fig. 1, phase II) as proposed by Cheng *et al*. (1994). Finally, the generated potential maps were evaluated to choose the optimum one by an efficiency index measure (Fig. 1, phase III), where the TOPSIS maps had the highest efficiency in the gold prospectivity mapping among all applied methods. Since both outranking methods along with the index overlay produced potential maps with close similarity in generating favorable zones, we could suggest with higher certainty that the SE portions of the Alut region should be investigated by the detailed ground-based exploratory techniques, relating probably to an orogenic gold mineralisation system. The detailed formulations of the most well-known variants of two outranking approaches of the VIKOR (i.e. conventional and adjusted, see Appendix A1) and the TOPSIS (i.e. conventional, adjusted and modified, see Appendix A2) for MPM (Fig. 1, phase II), can be found in previous works (Abedi and Norouzi, 2016; Abedi *et al*., 2016), where their implementation has been listed in several steps.

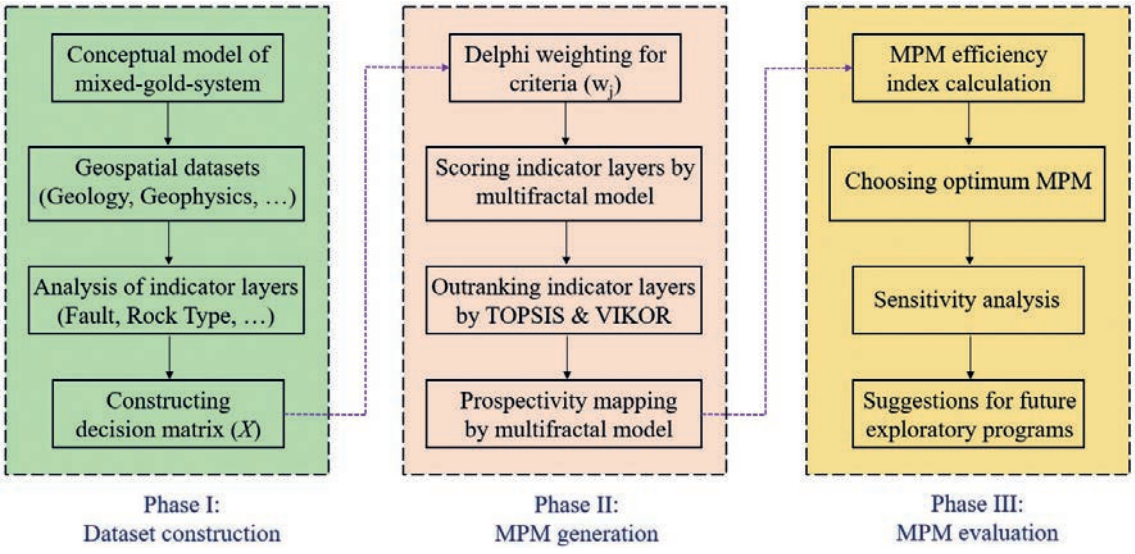

Fig. 1 - The general workflow followed in this study to generate MPM in gold exploration.

3. Geological setting of the Alut prospect zone in Iran

The Alut prospect zone is located in the Piranshahr-Sardasht-Saqez zone (PSSZ), NW Iran, to the north of the Sanandaj-Sirjan zone (SSZ). The SSZ is a complex and highly dynamic structural zone in Iran, located between two parallel zones of Zagros fold-thrust belt (that is bordered by the Zagros thrust) and Urumieh-Dokhtar (or Urumieh-Bazman) magmatic assemblage unit (UDMA), respectively in the SW and NE of its elongation. Indeed, the metamorphic and magmatic SSZ zone was considered as the suture between the Arabian and Eurasian plates (Dewey and Grantz, 1973), where its width is about 150-200 km with NW-SE trending thrusts involving sedimentary and

metamorphic Paleozoic to Mesozoic rocks (Alavi, 1994). Such rocks were intruded by Jurassic to early Eocene calc-alkaline magmatic rocks and middle Eocene gabbros (Masoudi, 1997). Most of the renowned and active gold mines in Iran have aligned along the SSZ, which hosts a wide range of gold deposit types in volcano-sedimentary series between lower green schist and amphibolite metamorphic rocks (Fig. 2). Researchers have stated that they are mainly orogenic and intrusion-related gold deposits (Aliyari *et al.*, 2012).

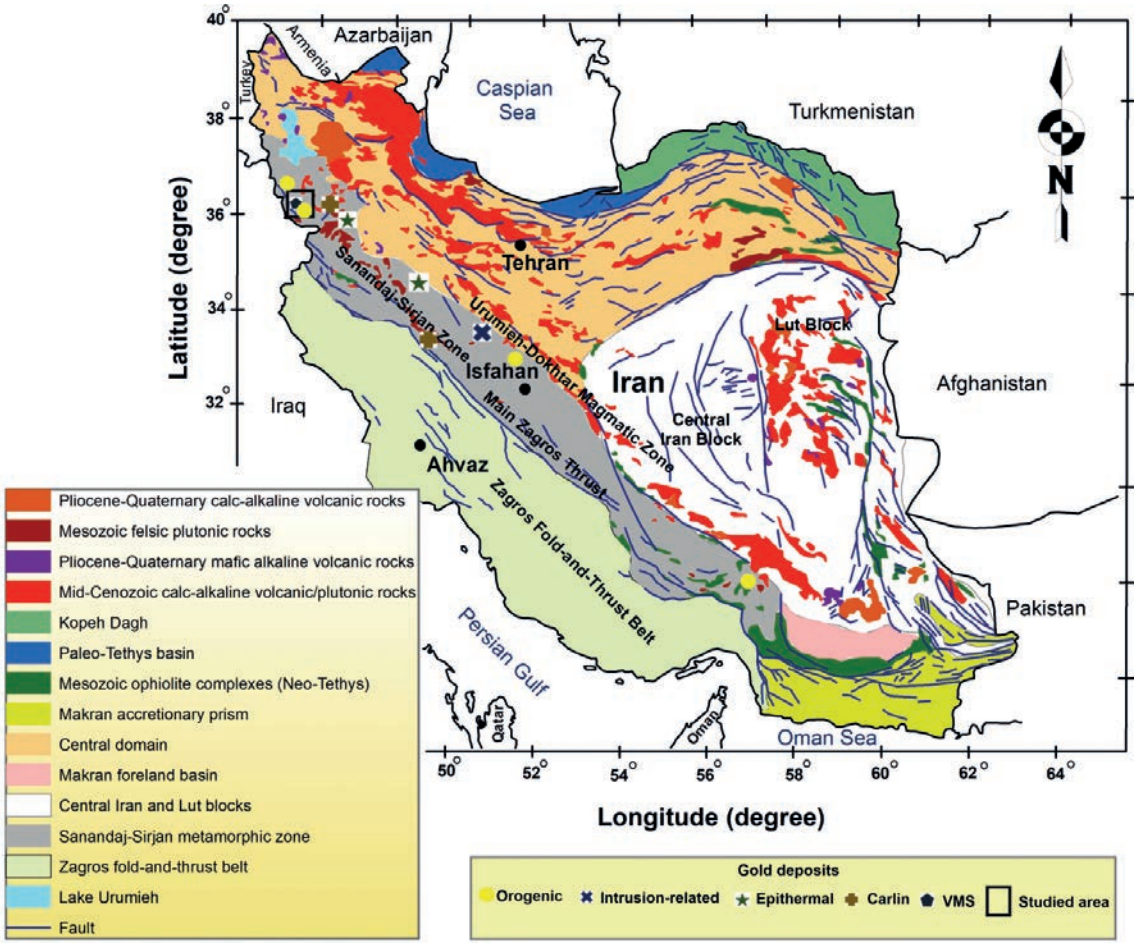

Fig. 2 - Location of the Alut prospect zone in the general geological map, on which the location of the main gold deposits in Iran have been superimposed (reproduced from Richards *et al.*, 2006). Note that orogenic, intrusion-related, epithermal, Carlin and Volcanic Massive Sulphide (VMS) deposits occur along the SSZ. Coordinate units are in degrees.

Most intrusion-related gold occurrences are associated with young structural setting, where gold-bearing occurrences are mostly isolated by normal faults. They underwent severe extensional tectonic activities in Middle to Late Tertiary. Note that the metallogeny of this highly potential gold zone (in particular orogenic gold indicators in northern portions of the SSZ, along with some epithermal gold and volcanogenic massive sulfide (VMS) deposits) was recently studied in terms of regional and crustal-scale processes by pointing to the minor links with tectonics (Moritz *et*

al., 2006; Richards *et al*., 2006). Roughly speaking, various types of gold occurrences such as intrusion-related, VMS, Carlin-type, epithermal, and mostly orogenic gold deposits, are available in this belt as a potentially mixed-gold-mineralisation system (Aliyari *et al*., 2009, 2012; Hosseini *et al*., 2015).

A substantial question is arising on the vague genetic model of the gold mineralisation in the SSZ, meanwhile there are also many uncertainties pertaining to the temporal and spatial relationship between the intrusions and gold mineralisation. Aliyari *et al*. (2012) stated that the gold mineralisation at some regions in the PSSZ was associated with the magmatic fluids, occurring within the granitoid intrusion units. In addition, gold occurrences have revealed clues about the thermal overprint. They also mentioned that the difference in metal constituents and the pattern of ore mineralisation probably pertain to various depths of occurrence or adjacency with magmatic feeders. Consequently, the metallogenetic evolution of this gold-content belt has simultaneously presented two systems of the orogenic- and intrusion-based models. Thickening the continental crust has given rise to an increasing number of gold occurrences in the SSZ unit of Cretaceous to Tertiary age. This works for most of the metamorphic gold mineralisation with the generic model of the orogenic system. Erosion level also plays an important role in these regions. Promising areas in association with the orogenic- and intrusion-based gold occurrences can be sought in severely eroded environments such as the metamorphosed volcano-sedimentary series along with the plutonic or sub-volcanic units (Aliyari *et al*., 2012; Hosseini *et al*., 2015). Fig. 3 shows a plausible genetic model for the formation of such gold mineralisation in the SSZ.

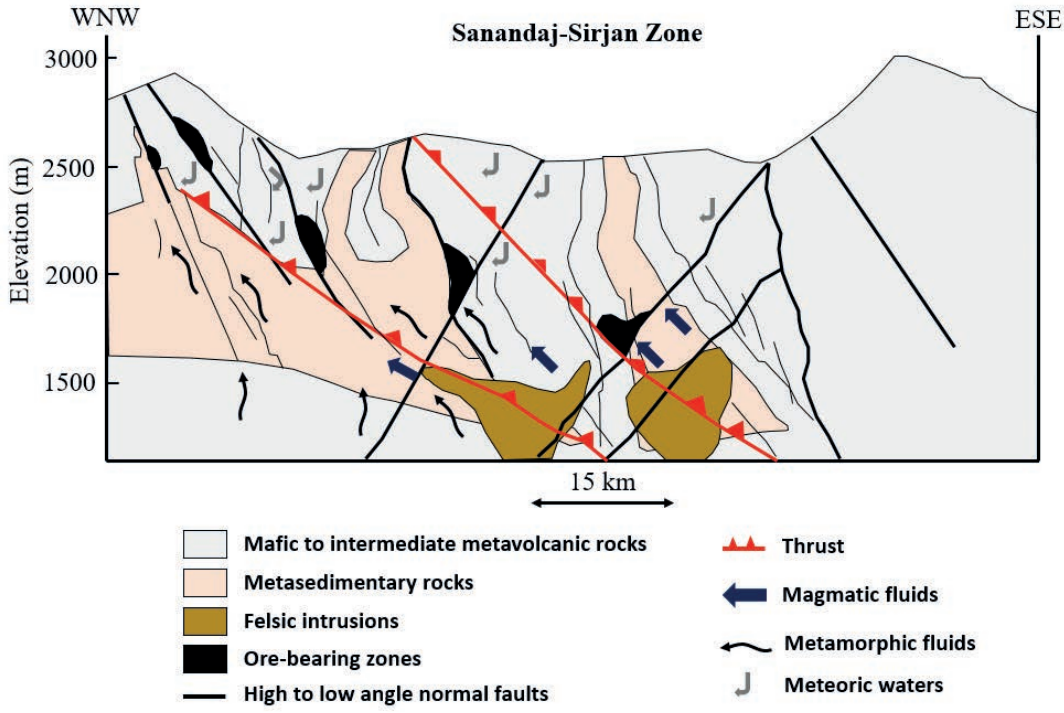

Fig. 3 - A plausible genetic model for the formation of orogenic and intrusion-related gold deposits by metamorphic fluids arising from the crustal rock devolatilisation in the SSZ and magmatic fluids from the Tertiary felsic intrusions (reproduced exactly from Aliyari *et al*., 2012).

The Alut district is located in the goldfield belt in the northern part of the PSSZ zone, hosted by mafic-intermediate metavolcanic and metasedimentary rocks. The detailed geological map of the Alut prospect with a scale of 1:100,000 is shown in Fig. 4. The age for most of the gold ore formations in the region of interest was Late Cretaceous to Early Tertiary, related to higher intensity of the metamorphism during the regional convergence and compression period. The associated intrusive bodies ranging in composition from tonalite porphyry, granite to diabase and volcanic activity, vary from acidic to basic. Since the background geologic setting of the SSZ unit is prone to gold-bearing systems, to investigate gold potential mapping, it is necessary to consider their lineament intersections reflecting the deep geological structures (Mohajjel *et al*., 2003; Aliyari *et al*., 2014; Hosseini *et al*., 2015; Mohammadzadeh and Nasseri, 2018).

Mafic to intermediate volcanic rocks, sericite and biotite schist, and granite intrusions were the main host rocks of the area, leading to gold-bearing mineralisation in narrow cross-cutting quartz-sulfide veins and veinlets at the Mirge Naghshine (or Alut deposit), Sheykh Choopan and Zaveh Kooh regions in the centre and east portions of the Alut sheet by an orogenic ductile to brittle shear zone controller.

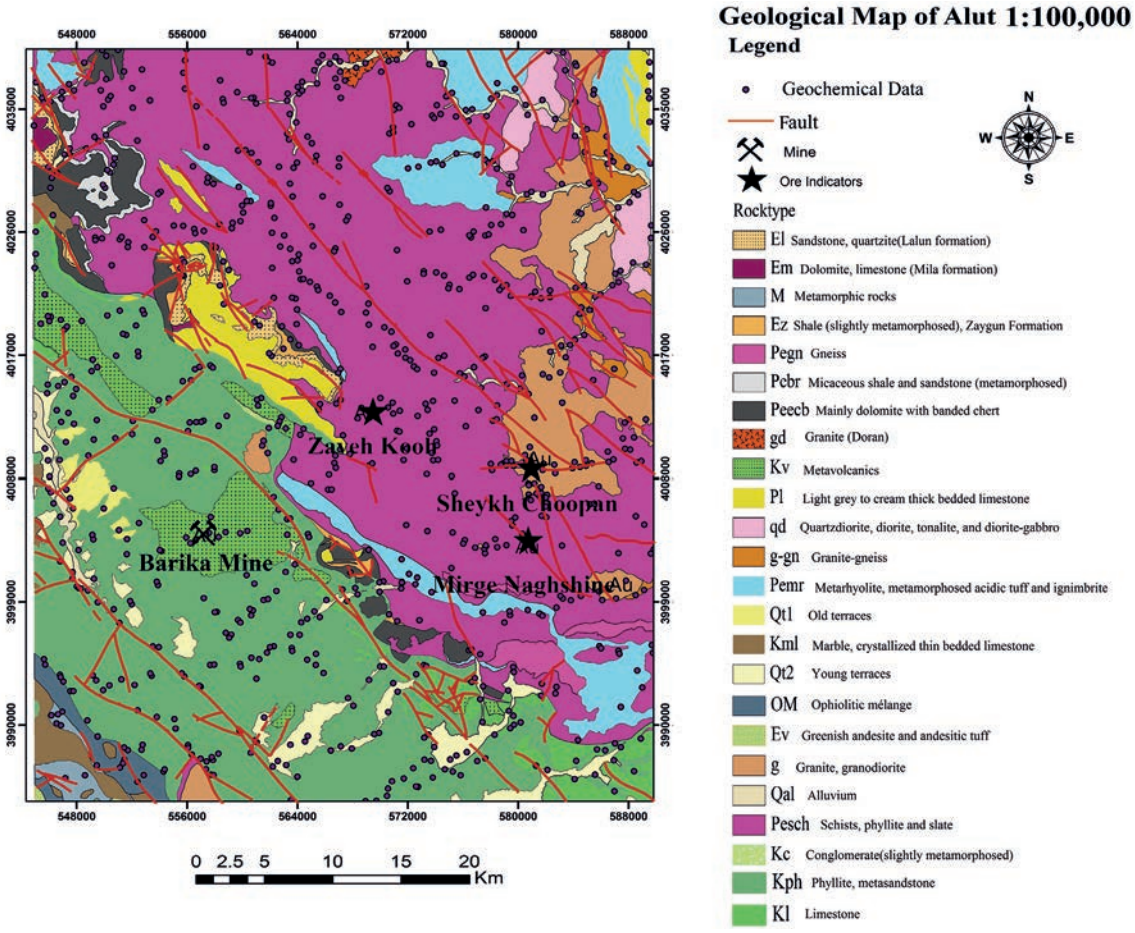

Fig. 4 - The geological setting of the Alut prospect zone, NW Iran (reproduced from the published map by the Geological Survey of Iran, GSI). The location of this region is shown in Fig. 2 with a square-shaped symbol.

These deposits are mostly controlled by deep-seated thrust or normal faults within the metamorphic geological setting. It is worth noting that quartz, sericite, carbonate, chlorite, and epidote were reported as the main alteration minerals for these occurrences. These dense gold-content quartz veinlets have frequently overprinted former disseminated gold-bearing zones (Aliyari *et al*., 2012). Sericite and silicic alterations, with distal assemblages of carbon and chlorite, are coincident with gold mineralisation in the Mirge Naghshine prospect zone (Asghari *et al*., 2018).

Meta-andesite and tuff host the Barika deposit as a gold-rich VMS in the Alut district within a back-arc tectonic setting. Gold mineralisation can be found in quartz sulfide, massive sulfide, sulfosalt, and barite zones. Quartz, sericite, pyrite, calcite, and albite were the common alteration minerals (Aliyari *et al*., 2012). In addition, regional metamorphism and deformation has given rise only to modification of the deposit properties, where the constituents were locally slightly redistributed within structural controllers (Yarmohammadi, 2006).

4. Geospatial data sets preparation

The following subsections briefly outline the procedure of extracting twelve indicator layers from a multi-disciplinary data set consisting of the geological, satellite imagery, geochemical and geophysical criteria. All these layers were categorised by the C-N multifractal method (Appendix A3) to assign appropriate scores of each category in preparation of the final MPM.

4.1. Geological indicators

According to the mixed systems of the Au-bearing mineralisation in the Alut prospect zone, the role of intrusion-related rocks and geological lineaments (faults, shear zones and contacts) were much more important than other factors. It has been noted that the intrusive rocks such as granite, granodiorite and metavolcanic rocks (first important group) were strongly related to the Au occurrences in this zone, in particular for the intrusion-related mineralisation (Hosseini *et al*., 2015). Moreover, granite and granite-gneiss rocks as the second important group were also associated with the mineralisation by assuming lower scores in this study. Table 1 summarises the importance of the rock units shown in Fig. 4 based on averaging the assigned scores to each rock type by the geoscientist decision makers from the Geological Survey of Iran (GSI). The Orogeny Au deposit is due to factors such as pressure to tensile deformation at the edges of convergent plates during orogeny. Therefore, structural controllers in the shear zones provide valuable information on the gold MPM procedure, where such environments generate corridors for circulating Au-content hydrothermal fluids, strongly altering the rock units and depositing Au ores. Researchers mentioned that mineralisation is closely coincident with first- and second-order faults, parallel and perpendicular to the SSZ, respectively (Mohajjel *et al*., 2003; Aliyari *et al*., 2009). Consequently, extracting the structural lineaments along with the altered regions in the mixed-system gold-bearing zones can yield to determining the Au-rich zones in the Alut district. Some multi-ring buffers were assumed around the main traces to consider the importance of vicinity areas to the fault systems that control the flow of the deep-seated hydrothermal fluids towards higher crustal levels. Fig. 5 shows the fault indicator map, in which the importance gradually decreases by moving at an interval of 50 m away from the centre. Table 2 shows the assigned scores to each interval distance.

Table 1 - The normalised scores of various rock types in the Alut prospect zone (assuming two types of gold-bearing system, orogenic and intrusion-related).

Rock ID	Rock Type	Score
E l	Sandstone, quartzite (Lalun formation)	0.20
E m	Dolomite, limestone (Mila formation)	0.15
E v	Greenish andesite and andesitic tuff	0.10
E z	Shale (slightly metamorphosed), Zaygun Formation	0.10
g	Granodiorite	0.90
g d	Granite Doran as Precambrian plutonism in Iran	0.70
g-gn	Granite-gneiss	0.70
K c	Conglomerate (slightly metamorphosed)	0.15
K l	Limestone	0.15
K ml	Marble, crystallised thin bedded limestone	0.15
K ph	Phyllite, metasandstone	0.45
K v	Metavolcanics	1.00
M	Metamorphic rocks	0.35
OM	Ophiolitic mélange	0.35
P l	Light grey to cream thick bedded limestone	0.15
PE br	Micaceous shale and sandstone (metamorphosed), Bayandor Formation	0.15
PE gn	Gneiss	0.15
PE mr	Metarhyolite, metamorphosed acidic tuff and ignimbrite	0.50
PE sch	Schists, phyllite and slate	0.55
PE-E cb	Mainly dolomite with banded chert (Soltanieh-Barut Formation)	0.20
Q al	Alluvium	0.04
Q t1	Old terraces	0.10
Q t2	Young terraces	0.20
qd	Quartzdiorite, diorite, tonalite, and diorite-gabbro	0.25

Table 2 - Scores assigned to the buffer zones around the faults.

Distance (m)	Score	Distance (m)	Score
50	0.95	300	0.5
100	0.90	350	0.4
150	0.80	400	0.3
200	0.70	450	0.2
250	0.60	>450	0.1

4.2. Satellite imagery indicators

The Advanced Spaceborne Thermal Emission and Reflection Radiometer (ASTER) remote sensor is a suitable tool for mapping hydrothermal alteration zones associated with gold deposits. It includes three separate subsystems of visible near-infrared (VNIR; bands 1-3 with 15 m resolution

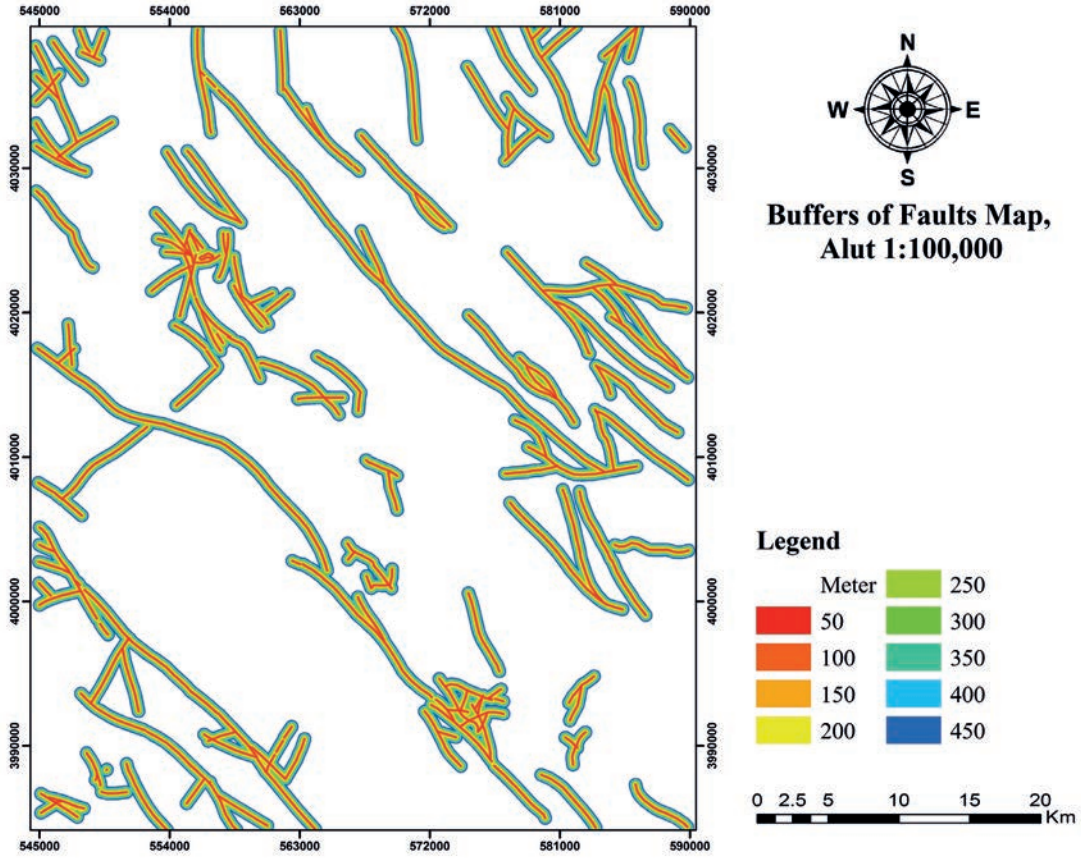

Fig. 5 - Fault indicator map in the Alut prospect zone.

and 0.4-1.4 μm wavelength), short-wave infrared (SWIR; bands 4-9 with 30 m resolution and 1.4-2.5 μm wavelength) and thermal-infrared (TIR; bands 10-14 with 90 m resolution and 8.0-14.0 μm wavelength) regions with 14 bands (Mars and Rowan, 2006; Mohebi *et al*., 2015). Alterations such as argillic, propylitic, phyllic, silicic, alunite, and jarosite, were closely related to the Au-bearing mineralisation systems in the SSZ (e.g. Almasi *et al*., 2014; Hosseini *et al*., 2015; Afzal *et al*., 2017). Due to the nature of the multi-system, Au-bearing mineralisation and its correlation with the hydrothermal fluids, the sought gold mineralisation is significantly affected by the argillic alteration. Propylitic alteration often generates in all types of magmatic and hydrothermal occurrences, but to a less extent in gold mineralisation systems. Since this alteration affects a huge area around the source in comparison to the others, it plays a powerful role in the reconnaissance stages. Although phyllic alteration is less significant than argillic in the Au exploration, it was practical because of its extension. In addition, most of the times the silicic alteration is formed in presence of the magmatic and hydrothermal fluids. Alunite minerals occurring in porphyry-type Cu and epithermal Au systems caused the acid-oxidizing status (Knight, 1977). They may be generated in case of weathered sulfides (Bladh, 1982), mostly observed in the top 60 m of ore-bearing systems with alunite-jarosite products (Morrison *et al*., 1987; Scott, 1990).

To prepare alteration indicators (i.e. argillic/propylitic/phyllic/silicic), the images of the ASTER satellite were analysed by the least square fitting (LS-Fit) method in ENVI software. Assuming

a linear band prediction using a least squares fitting technique, the LS-Fit method attempts to extract the regions of anomalous spectral response in input imagery data by comparison to a reference spectrum library. In fact, it calculates the covariance of the input data and the reference ones to predict the selected (or modelled) band as a linear combination of the predictor/input bands (Poormirzaee and Oskouei, 2010). This technique was used to extract the aforementioned altered areas. Then, the C-N multifractal method was applied to each alteration map (shown in Fig. 6) to categorise favorable zones associated with the probable Au mineralisation. Indeed, fractal curves facilitate assigning an appropriate score to each category within an alteration map. Table 3 presents the summary of all extracted threshold values for each alteration layer. Assuming the SWIR bands 4/5/7/8/9 as the input and the band 6 as the modelled one, the argillic alteration

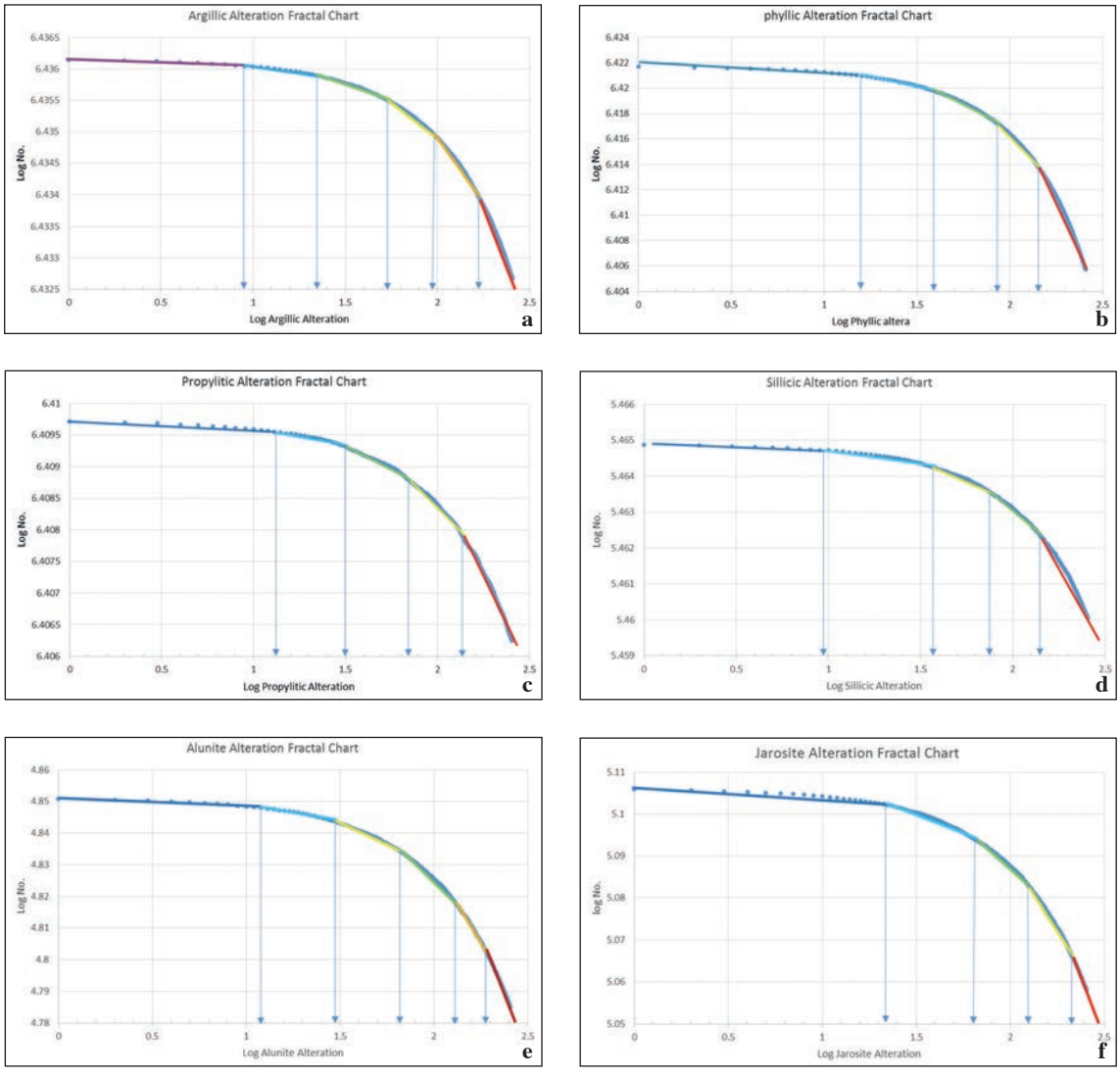

Fig. 6 - The C-N fractal-based curves for extracting appropriate thresholds to reclassify favorable zones in alteration maps. These alterations correspond to: a) argillic, b) phyllic, c) propylitic, d) silicic, e) alunite, and f) jarosite. The log-log plot presents the pixel numbers versus the threshold values.

was plotted. The alteration plot (Fig. 7a) shows that the argillic alteration covered the central and SE portions of the Alut district. The concentration of this alteration was observed around the boundary of the Barika and south of the Mirge-Naghshine in the meta-alkaline rocks, limestone, and metamorphic acidity tuff and meta-ryolite units. Also, it was spatially associated with schist, phyllite, and slate units. The centralisation of this alteration was more evident on the boundaries between the rock units, indicating the importance of geological contacts.

Table 3 - The normalised assigned scores to the various alteration layers after reclassification by fractal technique. RGB unit value is at an interval of 0-255.

Argillic		Alunite		Jarosite	
RGB unit value	Score	RGB unit value	Score	RGB unit value	0.9
0-43	0.9	200-255	0.9	131-255	0.9
43-85	0.7	129-200	0.7	65-131	0.7
85-128	0.5	65-129	0.5	24-65	0.5
128-170	0.3	29-65	0.3	10-24	0.3
170-213	0.2	10-29	0.2	0-10	0.1
213-255	0.1	0-10	0.1		
Phyllic		Propylitic		Silicic	
RGB unit value	Score	RGB unit value	Score	RGB unit value	Score
0-15	0.9	0-12	0.9	0-9	0.9
15-38	0.7	12-30	0.7	9-37	0.7
38-85	0.5	30-67	0.5	37-76	0.5
85-147	0.3	67-135	0.3	76-148	0.3
147-255	0.1	135-255	0.1	148-255	0.1

Assuming the SWIR bands 5/6/7/8/9 as the input and the band 4 as the modelled one, the phyllic alteration was plotted by the LS-Fit method. Phyllic alteration was commonly seen in granodiorite units, associated with the hydrothermal and epithermal gold mineralisation (Fig. 7b). In the centre of the Alut, it is located over the Mirge Naghshine, to the west of Sheykh-Choopan. The concentration of this alteration was controlled by metavolcanic, schist, and slate rocks, but in the NE and east of the map, the alteration was mainly due to granite, gneiss, and metarhyolite rocks. Although propylitic alteration is more common in the epithermal gold deposits, it was used as an indicator footprint because of its wide expansion and substitution in limestone rocks. Assuming the SWIR bands 4/5/6/7/9 as the input and the band 8 as the modelled one, the propylitic alteration was plotted. This alteration propagated over the entire area, but its enrichment was in the Barika, Mirge-Naghshine, and Sheykh Choopan regions (Fig. 7c). Some portions of this alteration were extended to the NE. The propylitic alteration was also observed in calcareous stones, granite, granite-gneiss, tuff, and crystalised limestone.

Assuming the TIR bands 10/11/13/14 as the input and the band 12 as the modelled one, the silicic alteration was mapped, where it was found in phyllite, schist, and slate rocks (Fig. 7d). Although this alteration has been detected in the south of the Alut district, it generally followed the faults trend along the NW-SE direction, parallel to the SSZ (Figs. 2 and 4). In spite of not

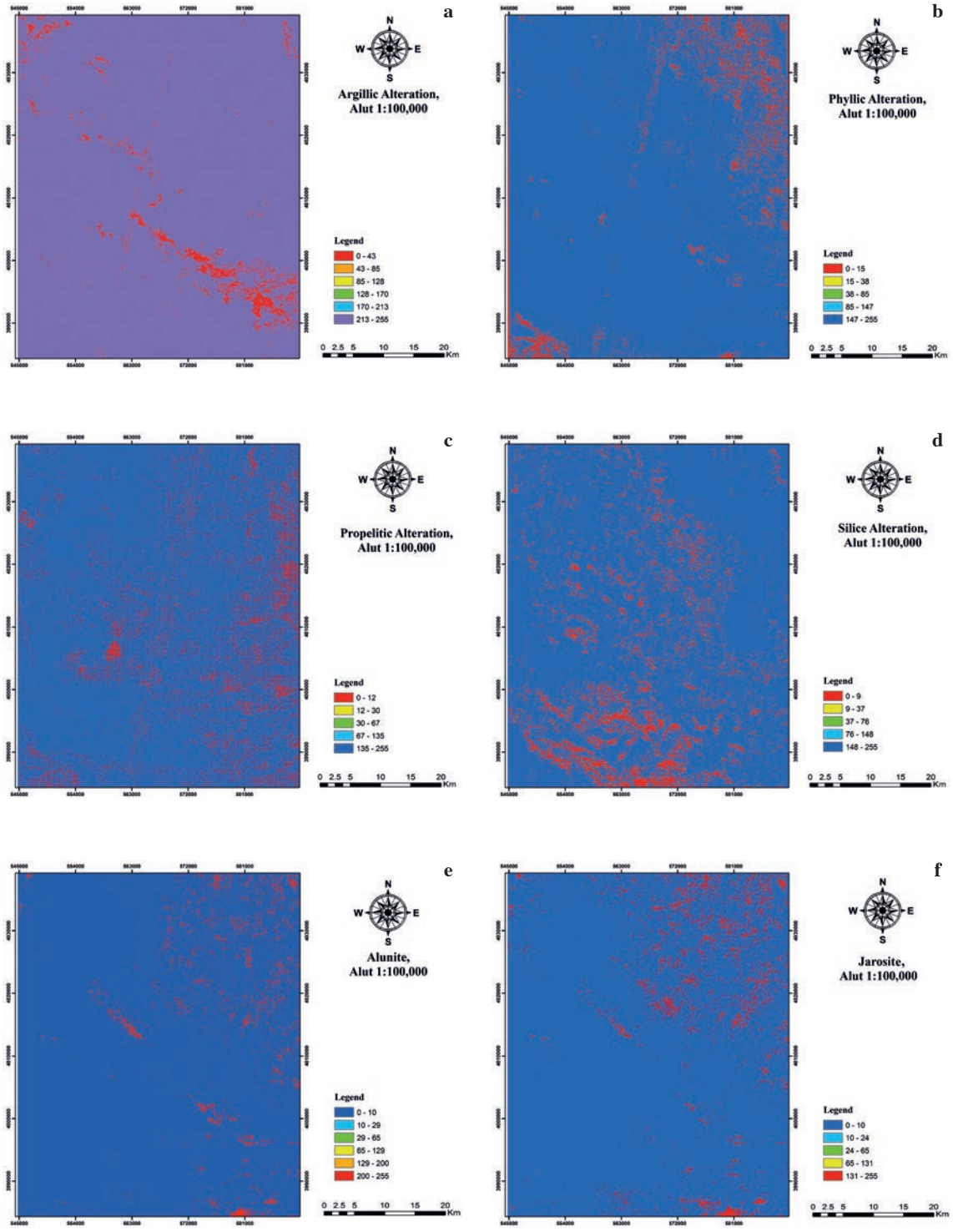

Fig. 7 - Various alteration maps in the prospect region namely: a) argillic, b) phyllic, c) propylitic, d) silicic, e) alunite, and f) jarosite. All units are in RGB colour system.

being closely related to the gold occurrences, the silicic alteration could indicate the importance of the faulted zones as a strong controller in the orogeny-type Au mineralisation.

In addition, spectral angle mapper (SAM) was applied to image alterations of the alunite and jarosite. This calculates the angle in spectral space (using the SWIR bands in this work) between pixels and a set of reference spectra (end members) for image classification based on the spectral similarity. Alunite alteration was observed in three main portions, in the centre of the map above the Barika border, in the SE below the Mirge-Naghshine, and in the NW regions. The phyllite, schist, and slate rocks, along with the limestone units, included this alteration in the centre and the SE, while the granite and granite-gneiss rocks contained it in the north. The jarosite expansion was similar to the alunite to some extent. The difference between these two was the extension of alteration in the north and south. Jorosite expanded more than alunite in the north, and in the south it was less diffuse. Alunite usually occurs in the high sulphidation epithermal deposits, namely an acidic environment, while jarosite is produced by weathering of the sulphides. Due to a higher correlation between the alunite and the gold mineralisation, the weight of this layer was assumed slightly higher than the jarosite. According to the high significance of these two minerals in gold exploration, the weights of these evidential layers were assumed high by the decision makers.

4.3. Geochemical indicators

In order to discover anomalous geochemical halos, 855 stream sediment samples were collected over the whole prospect region (Fig. 4). To extract the anomalies arising from the probable gold mineralisation, the multifractal method was used to separate favourable anomalous regions from the background. The samples were analysed in a laboratory for 20 elements by atomic absorption spectrophotometry. Statistical analysis was employed to exclude outliers from processing. Subsequent correcting of such noisy data was carried out based on the mean and the standard deviation of each element. The statistical characteristics of the main elements correlated partially with the Au element is shown in Table 4. The non-normal distribution of the Au concentration was evident based on the histogram, box-, and quantile-quantile (q-q) plots shown in Figs. 8a, 8b, and 8c, respectively. The q-q plot represents the concentration of Au in different quantiles against the standard normal distribution which provides better insights on the non-normal distribution of the Au concentration in this study.

Table 4 - The statistical characteristics of the main geochemical elements partially correlated with the Au.

Element	Min	Max	Mean	Median	Std. deviation	Skewness
Ag	0.01	0.22	0.103	0.10	0.0280	1.381
As	1.92	62.10	15.391	11.70	10.6120	1.429
Au	0.30	8.50	2.403	1.80	1.8070	2.100
Cu	13.00	68.00	35.650	35.00	9.3590	0.310
Mn	0.02	0.30	0.100	0.09	0.0457	1.666
Mo	0.14	6.20	1.466	1.19	1.0312	2.131
Sb	0.15	5.05	1.359	1.13	0.8580	1.592
Sn	2.10	6.90	3.619	3.50	0.7610	1.479
Ti	0.19	2.10	0.762	0.70	0.2910	1.177
W	0.09	3.94	1.417	1.25	0.7570	1.801

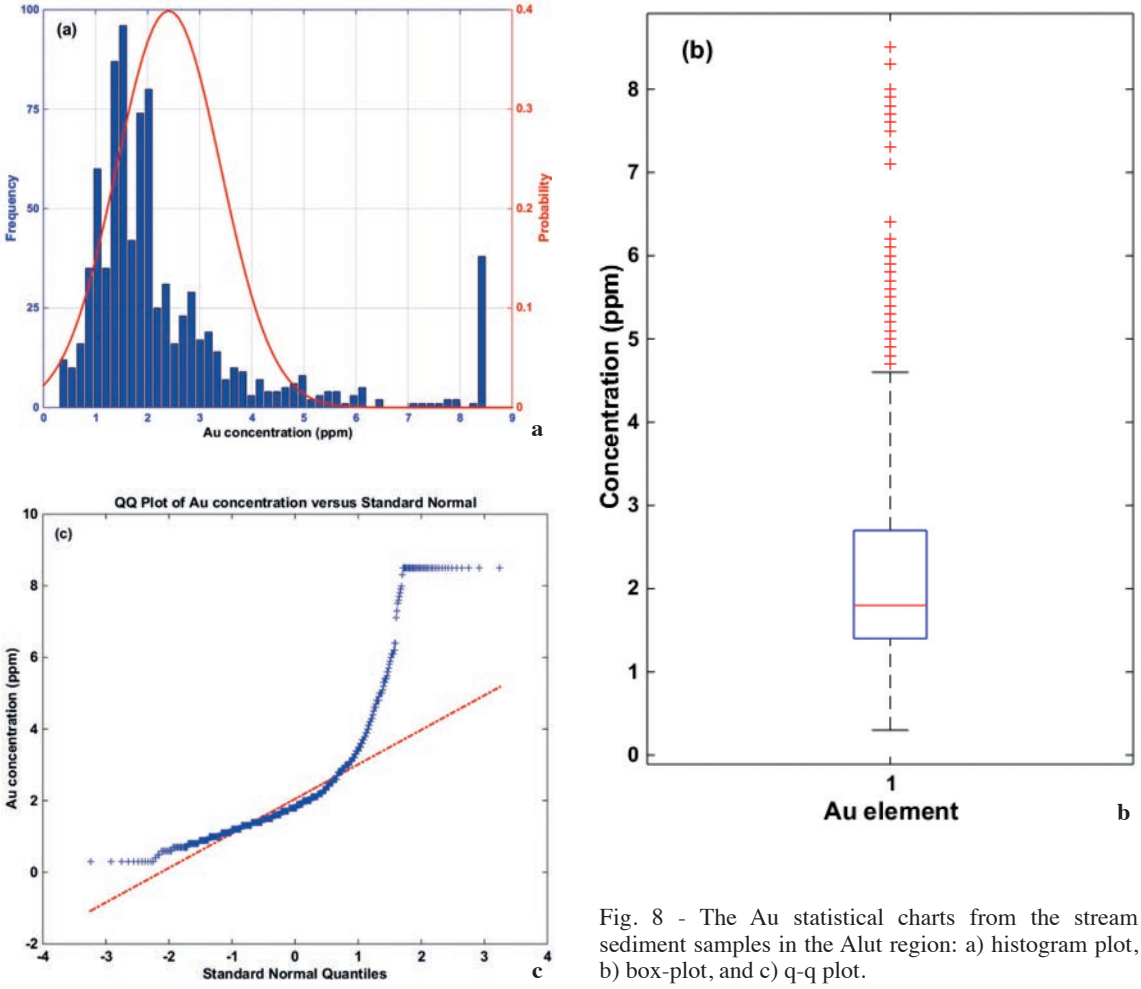

Fig. 8 - The Au statistical charts from the stream sediment samples in the Alut region: a) histogram plot, b) box-plot, and c) q-q plot.

Table 5 - The Spearman correlation among the CLR geochemical data samples.

Ag	1.000									
As	-0.451	1.000								
Au	-0.076	0.074	1.000							
Cu	0.231	-0.165	-0.016	1.000						
Mn	0.105	-0.041	-0.241	0.006	1.000					
Mo	0.014	-0.192	0.022	-0.048	-0.506	1.000				
Sb	-0.226	0.232	0.069	-0.053	-0.462	0.273	1.000			
Sn	0.405	-0.389	-0.190	-0.019	0.091	-0.118	-0.475	1.000		
Ti	0.024	-0.196	-0.030	-0.132	-0.118	0.159	-0.020	0.094	1.000	
W	-0.264	-0.027	-0.074	-0.193	-0.259	0.098	-0.051	0.129	-0.099	1.000
	Ag	As	Au	Cu	Mn	Mo	Sb	Sn	Ti	W

Centred Log-Ratio (CLR) transformation was used to normalise geochemical elements (Aitchison, 1986), while the calculated Spearman's ranked correlation coefficient (Appendix A4) among the transformed data were trivial (Table 5). These data were the inputs of the factor analysis to extract the main geochemical factor associated with the Au mineralisation. Non-rotated factors could not show all correlations properly, since many variables are related to one or many factors, so to prevent this, a rotated matrix should be used. Differences in the chemical properties of the elements, as well as the nature of the factor analysis method in which the whole matrix of data is used, make it possible to construct the factors with fewer effective elements. In order to improve the output of the multivariate analysis, a staged factor analysis (sequential procedure) was used to infer the best multi-element factor associated with the mineralisation. The basis of the staged factor analysis is that the element or elements will be omitted if their loads are less than a predefined threshold value after performing each iteration. Factor analysis will be iterated again until all elements have a loading above a predefined threshold value. The stage factor analysis is done in two major phases; 1) the elimination of elements that are not involved in any factors, and 2) extraction of several anomalous elements closely related to the target in order to identify the mineralisation types and to achieve reliable factor weights (Borovec, 1996; Van Helvoort *et al*., 2005; Yousefi *et al*., 2014).

In this work, the factor analysis was applied to all 20 elements in three stages. The threshold loading was considered equal to 0.6. According to the aforementioned rule, the elements with loading value lower than 0.6 were eliminated in the first stage (i.e. B, Ba, Bi, Co, Cr, Ni, Pb, Zn). In the second stage, Be and Hg were omitted as well. At the end, Ag, As, Au, Cu, Mn, Mo, Sb, Sn, Ti, and W elements remained. The main characteristics of these trace elements are summarised in Table 4. The fifth component of the staged analysis corresponded to the anomalous Au zones (Table 6), where the load of the Au was maximum (0.965) with partial correlation with As, Mn, and Mo elements. The geochemical data analysis of the trace elements in the Alut was a painstaking work, due to 1) the non-normal nature of their probability density function of the Au, 2) too much censored data, and 3) the existence of outliers as well. Among various developed fractal-based

Table 6 - Third stage of sequential factor analysis for CLR data, where a fifth component is chosen as a multi-element geochemical attribute with higher loading values.

	Component				
	C1	C2	C3	C4	C5
Ag	0.698	-0.037	0.359	0.244	0.029
As	-0.799	-0.149	-0.035	0.071	0.125
Au	-0.072	0.052	0.077	0.000	0.965
Cu	0.198	0.075	0.307	0.693	-0.058
Mn	0.064	-0.787	0.249	0.005	-0.319
Mo	0.144	0.813	-0.067	0-.096	-0.115
Sb	-0.499	0.641	0.215	0.040	-0.029
Sn	0.715	-0.237	-0.352	-0.147	-0.022
Ti	0.229	0.162	0.223	-0.794	-0.058
W	0.017	0.152	-0.896	-0.009	-0.072

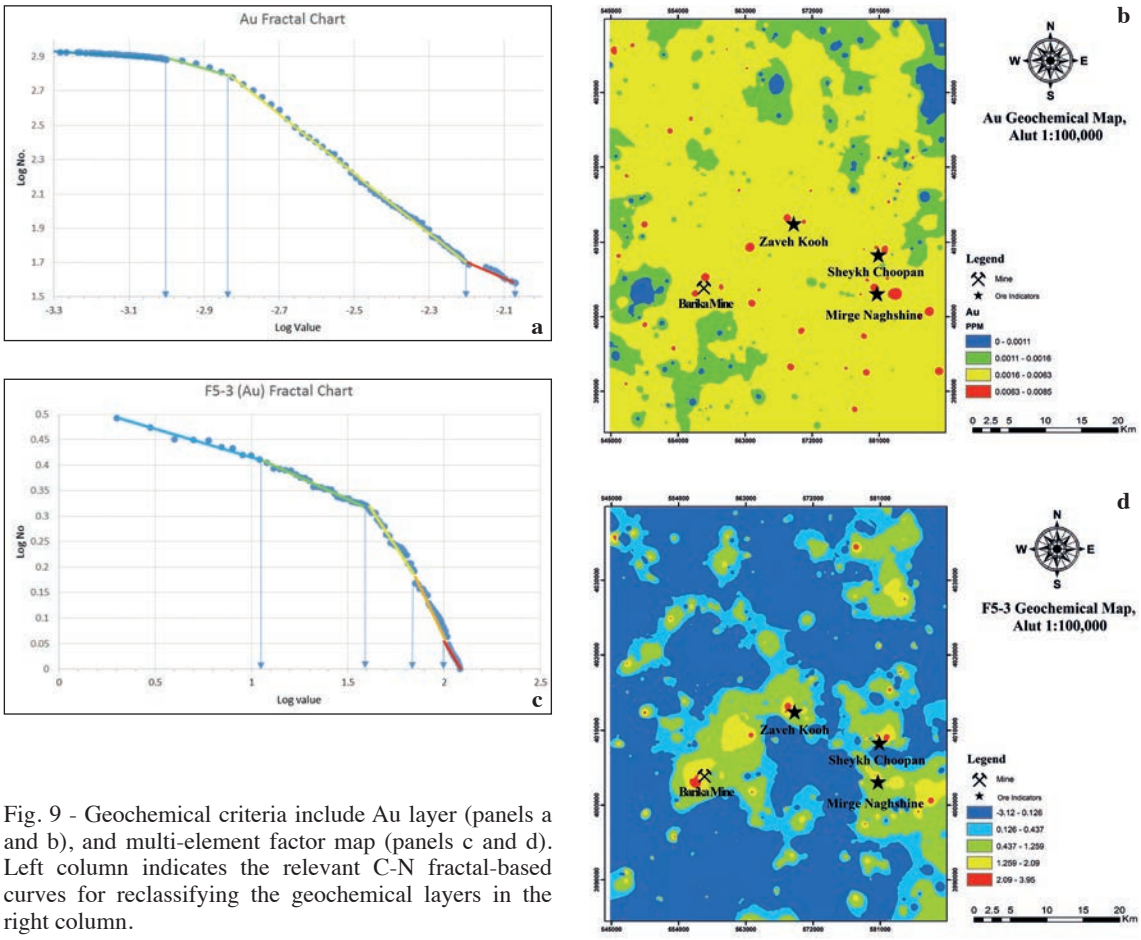

Fig. 9 - Geochemical criteria include Au layer (panels a and b), and multi-element factor map (panels c and d). Left column indicates the relevant C-N fractal-based curves for reclassifying the geochemical layers in the right column.

Table 7 - The normalised assigned weights to the geochemical layers after reclassifying by fractal technique.

Au Anomalies		Au Factor	
Range (ppm)	Score	Range	Score
0.0000-0.0011	0.1	-3.120-0.126	0.1
0.0011-0.0016	0.3	0.126-0.437	0.3
0.0016-0.0063	0.6	0.437-1.259	0.5
0.0063-0.0085	0.9	1.259-2.090	0.7
		2.090-3.950	0.9

approaches, the C-N multifractal version (Appendix A3) does not need to go through any pre-processing of the geochemical data (Hassanpour and Afzal, 2013). Therefore, by using the C-N method on the Au and Au factor maps (Table 7), the geochemical indicators were generated by the inverse distance weighted (IDW) interpolation method (Fig. 9). The produced Au factor map was much more closely matched with the previous known gold occurrences in the Alut compared to the single element Au map.

4.4. Geophysical indicators

Airborne geophysical surveys are advantageous tools in the reconnaissance stages of exploration programs by providing notable pieces of information about various natural resources such as mining, oil, geothermal, and environment. In particular, for mineral occurrence exploration, an airborne magnetometry survey can delineate promising environments that control the gold mineralisation such as the geological lineaments (faults, contacts, shear zones) and the intrusion-related magmatic units. Such collected information can be used to design an exploratory geospatial data set in MPM (Carranza and Sadeghi, 2010; Abedi *et al*., 2015).

Since the mixed systems of the orogenic and intrusion-related gold mineralisation have dominated the Alut, to localise the intrusive magmatic units and geological lineaments as a controller of the Au mineralisation, airborne magnetometry data could enhance the traces and borders of such sought structures. Here, 2500 data points were resampled from the aeromagnetic data set of Iran to generate a magnetic map over the prospect zone. The airborne magnetometry survey was supervised by the GSI with a 7.5 km line spacing along N-S direction. The reduced-to-pole (RTP) transformation was used to set the Earth's magnetic field inclination along the magnetic pole giving rise to positioning a positive pole over causative magmatic sources. The RTP generates a symmetric pattern of the magnetic signal, which facilitates the interpretation of the magnetic anomalies (Abedi and Oskooi, 2015; Oskooi and Abedi, 2015). According to the RTP map (Fig. 10b), there was an anomaly region in the SW of the Alut map which could be expressed as sources related with the deep-seated structural lineaments. The Tilt angle map, as a balanced vertical derivative of the magnetic field (Miller and Singh, 1994), could help to extract the traces of shallow structural lineaments as well. Compared to the RTP output, the Tilt map could better present the elongation of these structures, parallel to the SSZ. In particular, it delimited the borders of an orogenic-based gold-bearing zone extending from the centre to the SE portions of the area. By applying the fractal on these maps (Figs. 10a, 10c, and Table 8), they were incorporated in the data sets as geophysical indicators for the final preparation of the prospectivity map.

Table 8 - The normalised assigned scores to the geophysical layers after reclassifying by fractal technique.

RTP		Tilt Angle	
anomaly range (nT)	Score	Anomaly range (radian)	Score
-101.40-6.03	0.1	-1.57-0.16	0.1
6.03-19.96	0.2	0.16-0.48	0.3
19.96-40.74	0.3	0.48-0.96	0.5
40.74-53.71	0.4	0.96-1.32	0.7
53.71-131.83	0.5	1.32-1.56	0.9
131.83-208.96	0.7		
208.96-263.00	0.9		

5. MPM procedure

Exploratory data sets consisted of three main evidential criteria of the geology (surface studies and remote sensing), geophysics (magnetometry) and geochemistry. A group of experts in the field of gold exploration, mostly from the GSI with various disciplines in mineral exploration (i.e.

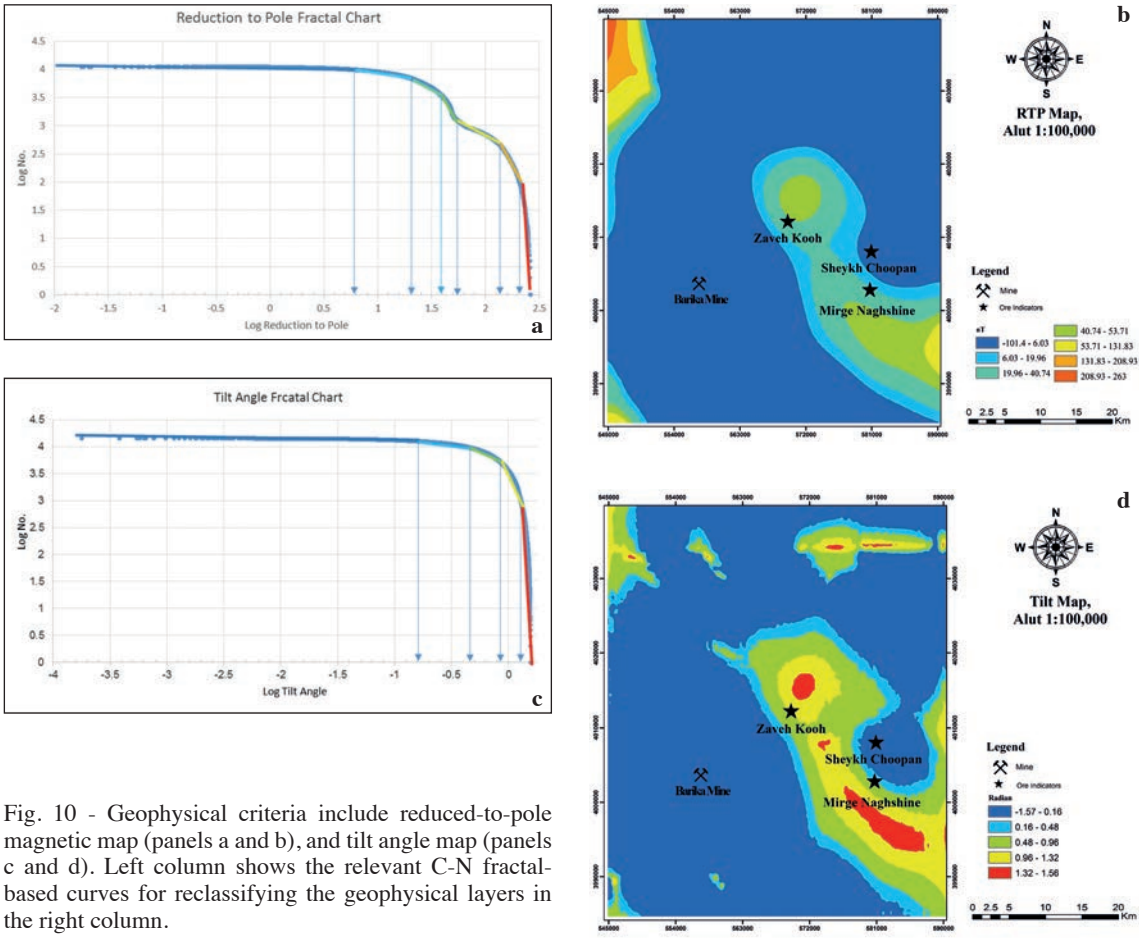

Fig. 10 - Geophysical criteria include reduced-to-pole magnetic map (panels a and b), and tilt angle map (panels c and d). Left column shows the relevant C-N fractal-based curves for reclassifying the geophysical layers in the right column.

geologists, geochemists, and geophysicists), was chosen to guide this project. Twelve sublayers (indicator/evidential layers), in which each one represented favourable zones responsible for the mineralisation, were prepared to be integrated by two well-known outranking methods of the TOPSIS and VIKOR. The decision tree shown in Fig. 11 indicated that the MPM procedure contained: 1) two layers of the Tilt angle and the RTP maps (the geophysics criterion), 2) two layers of the fault and rock type maps (from the surface geology), 3) six alteration layers of argillic, phyllic, propylitic, silicic, alunite, and jarosite (extracted from the satellite imagery data), and 4) two layers of the geochemical Au concentration and the Au factor maps (derived from processing the stream sediment data). The Delphi method, a well-known and popular weighting method, was used to assign the normalised weight of each indicator in this study (Gupta and Clarke, 1996; Linstone and Turoff, 2002; Skulmoski *et al.*, 2007). To simplify the procedure of determining sub-optimal weights of the indicator layers and criteria, a sample table like Table 9 was distributed among all decision makers to assign appropriate weights (in a scale of 0 to 1) to each layer based on their experience towards MPM in gold exploration. Averaging and normalising the assigned weights by the decision makers (about 30 members) such that the summation is equal to one ($\sum_{j=1}^{m} w_j = 1$), Table 9 summarises the final assigned weights, superimposed on the decision tree

as well (Fig. 11). All maps were transferred from vector to raster cells with dimensions of 200 m in both easting and northing directions. The final geospatial data sets constituted of a database of 60,827 rows and 12 evidential layer columns (i.e. the *X* decision matrix in Appendices A1 and A2).

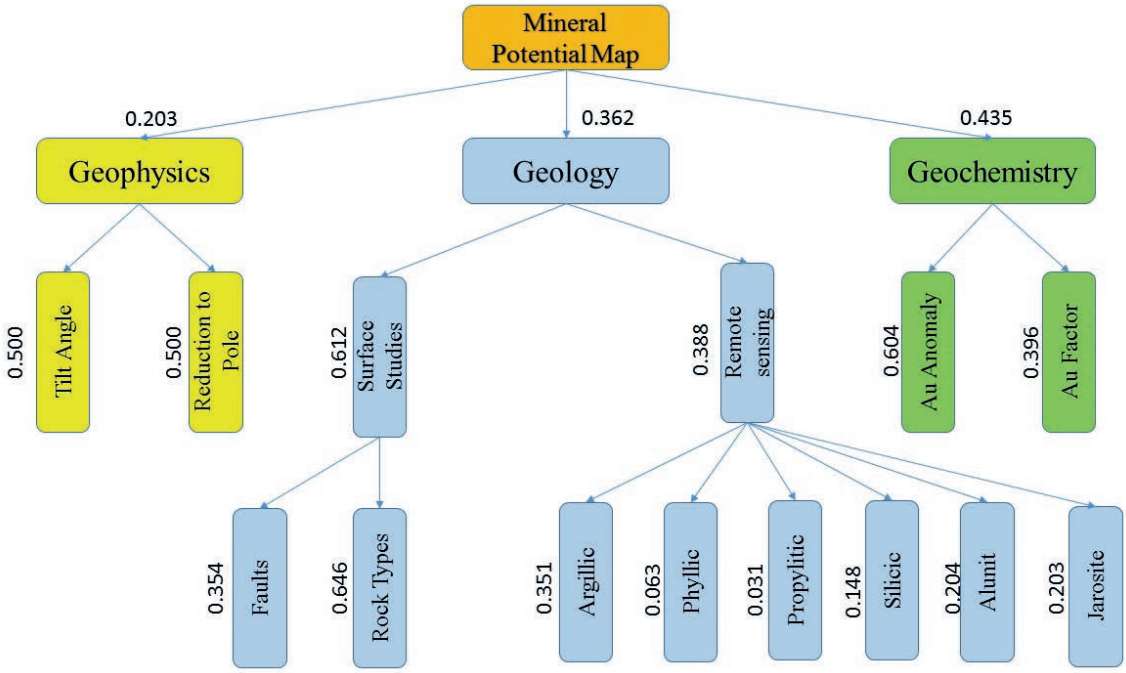

Fig. 11 - Decision tree flowchart for generating final MPM, on which the normalised weight of each evidential layer has been superimposed.

Table 9 - The normalised weight of each criterion in the final prospectivity map acquired from a group of geoscientist decision makers.

Layers	Weight	Sub-layer	Weight	Criterion	Weight	Final weights
Geology	0.362	Surface studies	0.612	Faults	0.354	0.079
				Rock types	0.646	0.143
		Remote sensing	0.388	Argillic	0.351	0.049
				Jarosite	0.203	0.029
				Alunite	0.204	0.029
				Propylitic	0.031	0.004
				Phyllic	0.063	0.009
				Silicic	0.148	0.021
Geochemistry	0.435	Stream sedimentary	1.000	Au	0.604	0.263
				Au factor	0.396	0.172
Geophysics	0.203	Magnetic	1.000	Tilt angle	0.500	0.101
				RTP	0.500	0.101

To produce the final MPM, two novel outranking approaches were employed. The C- and A-VIKOR were taken into account to integrate twelve evidential layers by incorporating their normalised weights derived from the Delphi method. Fig. 12 presents the potential maps, while the conventional C-A multifractal model was used to classify the area into favorable zones associated with the Au mineralisation. According to the results, both VIKOR maps indicated some high potential zones (plotted in red color) consistent with the previous active mine (e.g. Barika) and ore occurrences (Zaveh Kooh, Sheykh Choopan, and Mirge Naghshine). Three versions of the TOPSIS method were also used to generate final potential maps shown in the right column of Fig. 13. The C-A multifractal method (the left column of Fig. 13) extracted the highly favorable potential zones, probably responsible for the Au mineralisation (shown in red color in all maps). All TOPSIS maps showed a very good correlation with the previous mine and ore occurrences in the area as well.

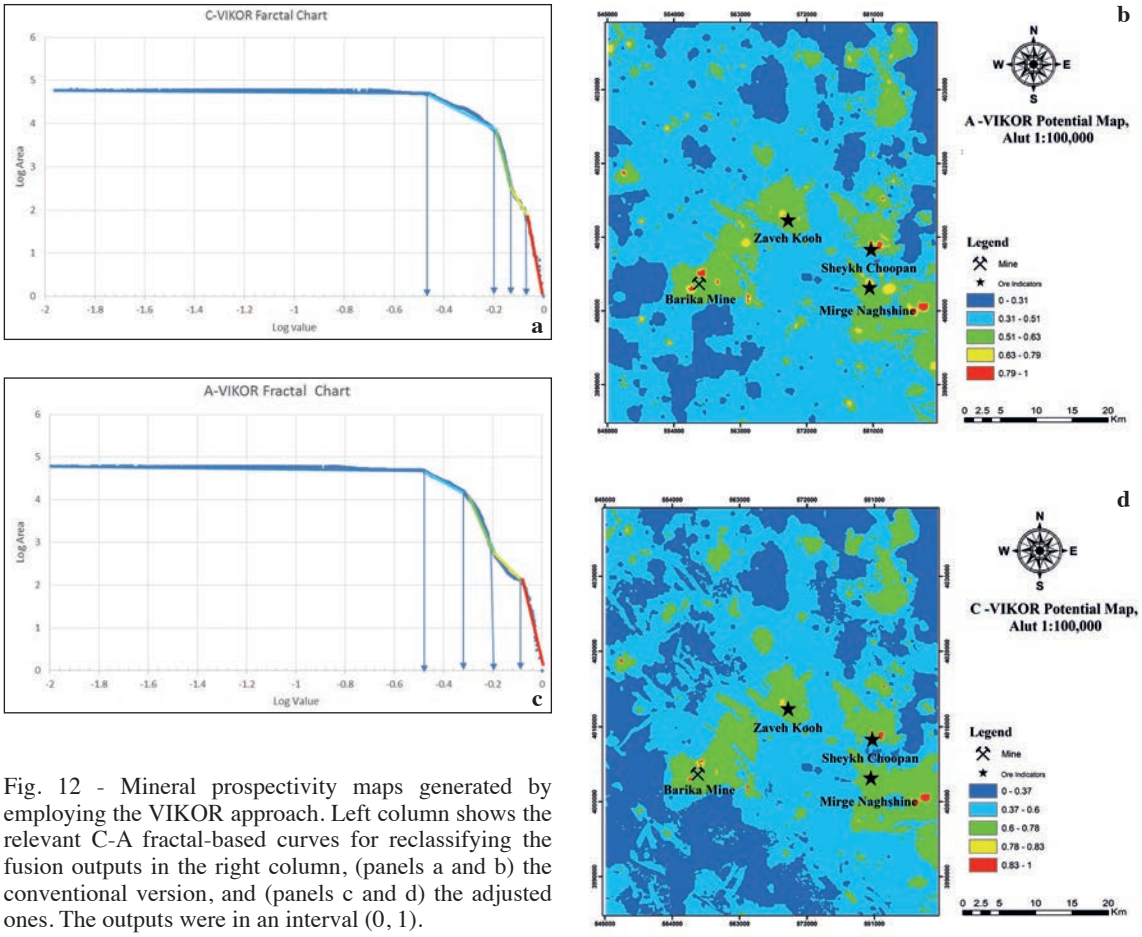

Fig. 12 - Mineral prospectivity maps generated by employing the VIKOR approach. Left column shows the relevant C-A fractal-based curves for reclassifying the fusion outputs in the right column, (panels a and b) the conventional version, and (panels c and d) the adjusted ones. The outputs were in an interval (0, 1).

Since various MPM techniques usually lead to different prospectivity maps, simultaneous consideration of several generated maps can reduce the uncertainty arising from each approach (Abedi *et al*., 2017). Here, five generated maps from developed outranking approaches enhanced two potential regions (in red color) distinguished at the SE of the Mirge Naghshine. The outputs

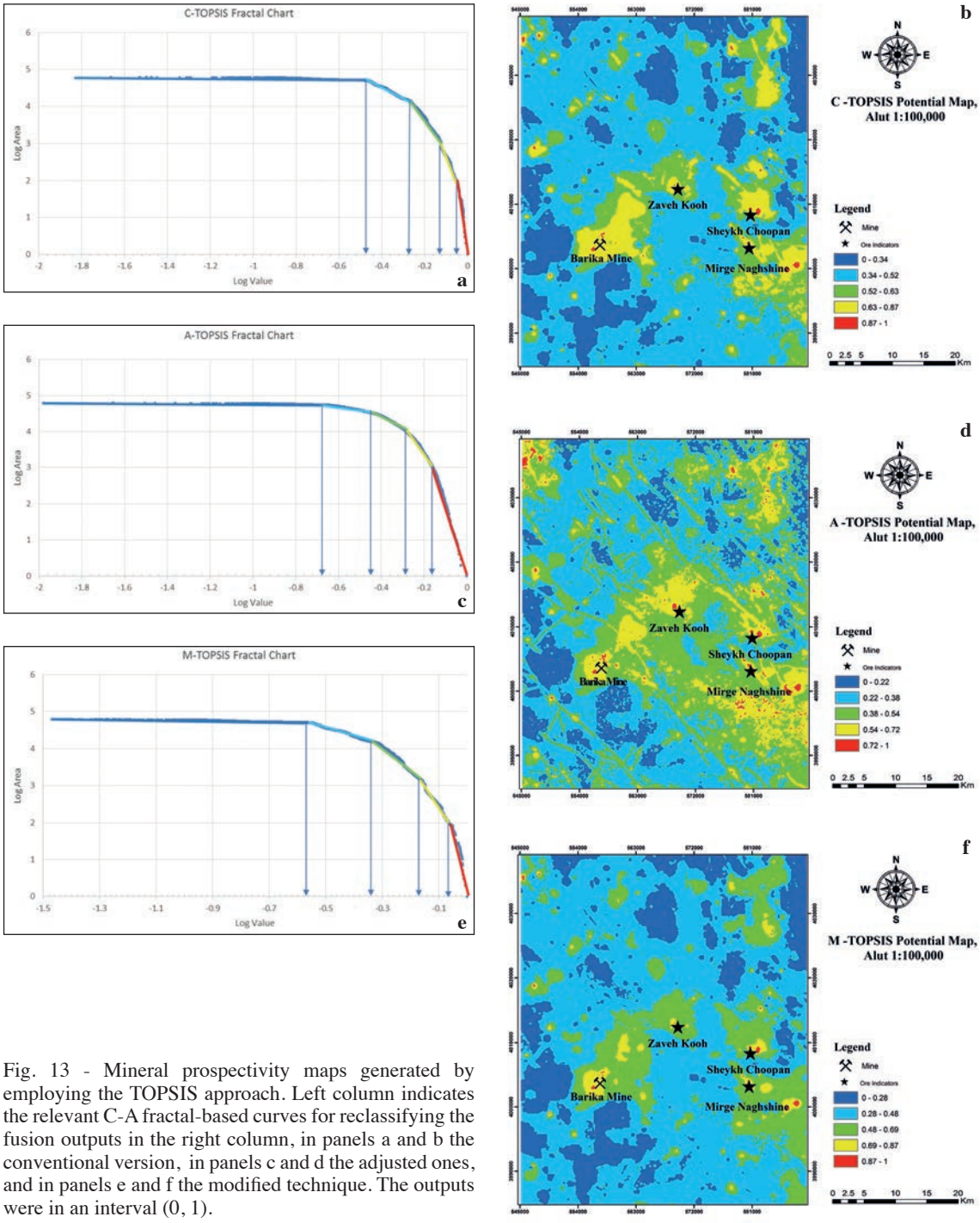

Fig. 13 - Mineral prospectivity maps generated by employing the TOPSIS approach. Left column indicates the relevant C-A fractal-based curves for reclassifying the fusion outputs in the right column, in panels a and b the conventional version, in panels c and d the adjusted ones, and in panels e and f the modified technique. The outputs were in an interval (0, 1).

were also compared to the fusion map derived from the multi-class index overly technique, where its final potential map was reclassified by the C-A multifractal approach (Fig. 14). This map has also localised these zones, but the portions of favorable regions were much bigger than the outranking methods.

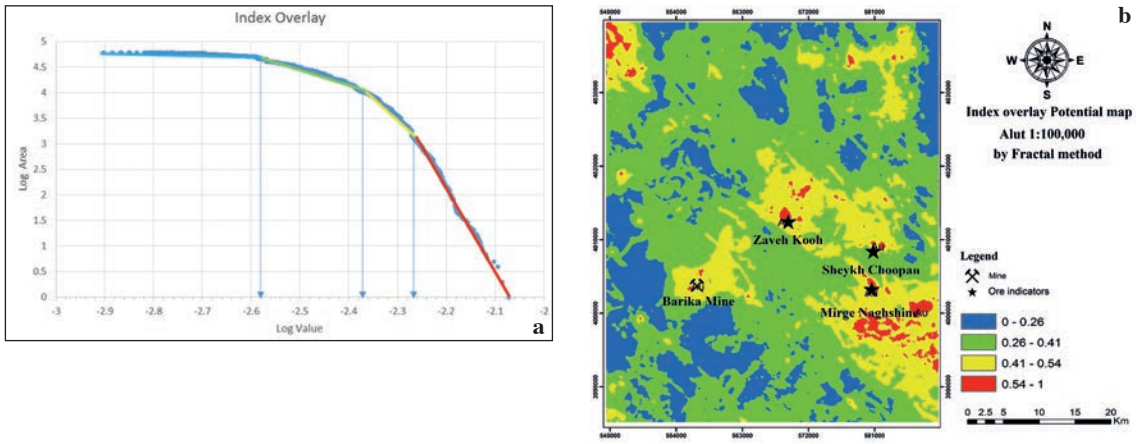

Fig. 14 - Mineral prospectivity map generated by the multi-class index overlay approach. Left column shows the relevant C-A fractal-based curve for reclassifying the fusion output in the right column. The outputs were in an interval (0, 1).

Lower predicted area (f_1), along with higher ore prediction rate (f_2), are two essential factors that are generally used in assessing the generated MPMs. An efficiency index (E.I.), proposed by Abedi *et al*. (2016), was utilised here to evaluate the performance of each applied techniques:

$$\text{E.I.} = w_1\,(100 - \text{predicted area }\%) + w_2\,(\text{ore prediction rate }\%) = w_1 f_1 + w_2 f_2 \qquad (1)$$

where $\sum_{i=1}^{2} w_i = 1$, and w_i denotes the relative weight of each factor in MPM evaluation. These factors are calculated through the ratio of the potential area to the total area, and the number of predicted ores over all ore numbers. Assuming relative weights equal to 0.5, higher output reveals a better performance of the applied technique (Abedi *et al*., 2016).

The MPM E.I. was calculated in this work for all applied methods (Fig. 15), where the TOPSIS attained the highest values (99.9% for the conventional and modified versions). It revealed that this outranking approach had higher accuracy compared to the VIKOR and partial superiority to the

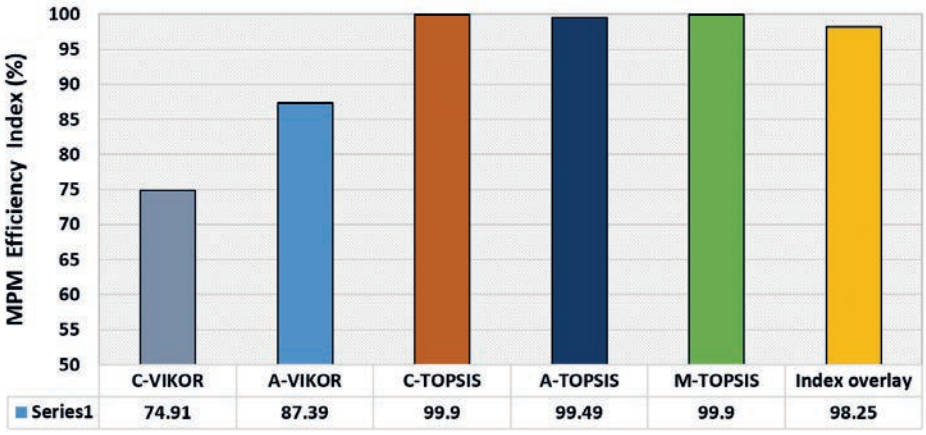

Fig. 15 - The MPM efficiency index for all applied algorithms showing the superiority of the TOPSIS method.

index overlay. Of note is that all methods indicated similar favorable gold occurrences at the SE regions in the Alut, mostly controlled by the orogeny system. Further exploratory investigations like ground-based geophysical survey and drilling are envisioned to determine the mining potential of these zones. The exploratory results at these prospect zones are confidential at present, where traces of gold mineralisation are evident in shear zones as the main structural controller.

The diversity of incorporated indicator layers in preparation of the MPM is a critical challenge among decision makers, where the numbers of layers may change from one case to another even in a similar mineralisation system. To evaluate the importance of twelve indicators in this study, sensitivity analysis of the MPM was carried out. Leave-one-out method was performed in which each indicator layer or each criterion (i.e. the geophysics, geology, and geochemistry) was excluded in the final preparation of MPM. Assuming the C-TOPSIS output as the one with the highest E.I., the potential maps were generated by leaving out each layer/criterion through this methodology. Fifteen potential maps were plotted versus the C-TOPSIS map (Fig. 13b, generated with 12 indicators). Fig. 16 shows these outputs against the one with all twelve layers. The slope of the scatter plots would be equal to one in cases that the new generated potential map has the lowest dependency on the excluded layer in the MPM procedure. The geochemical Au layer had the highest deviation (with a slope of 0.6824) from the C-TOPSIS MPM when it was left out of the data integration. This deviation was also high for the Tilt angle, rock type, Au factor and fault as well. Indeed, it showed the importance of these layers in preparing the final prospectivity map in the gold exploration. Among the three criteria of the geology, geophysics, and geochemistry, excluding geochemistry criteria had the highest deviation from the optimum generated MPM in this study.

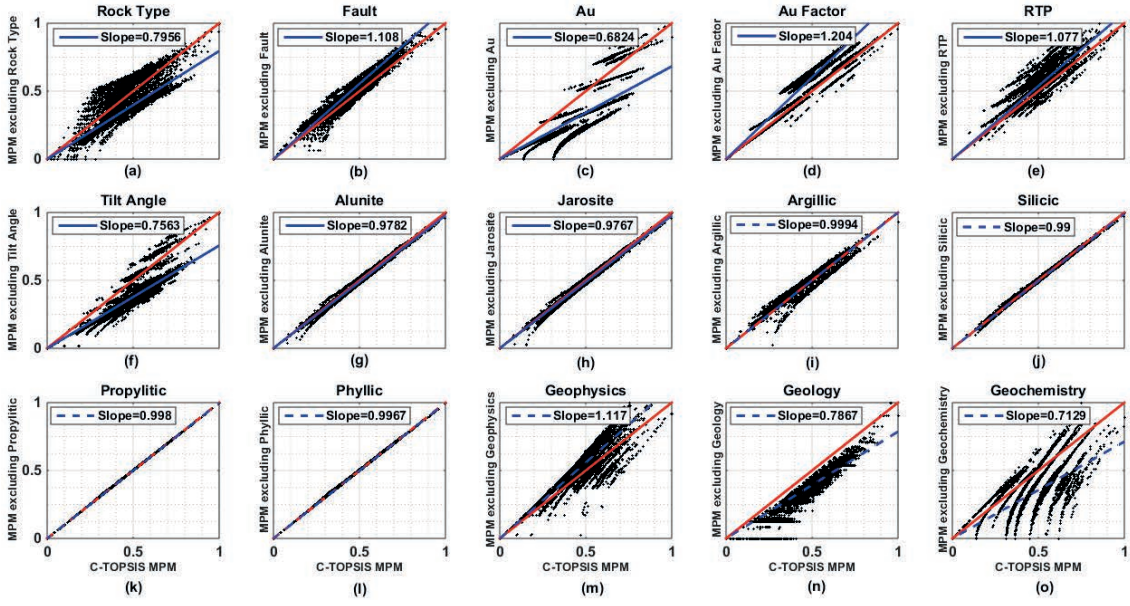

Fig. 16 - Sensitivity analysis of the MPM process by the leave-one-out method in which each indicator layer and three criteria of the geophysics, geology, and geochemistry were excluded in the final implementation of the C-TOPSIS method. The comparison was performed with the C-TOPSIS MPM result by considering all layers with highest efficiency index of 99.9%.

6. Conclusion

In this paper, by adapting outranking approaches and incorporating fractal concepts, a complicated mineral system of gold deposition processes in a complex goldfield was broken down into classes of exploration evidence data in order to better understand the natural phenomenon, namely gold mineralisation. Different prospectivity models were, then, generated to define reliable exploration targets. Evaluation of the functionality of the method proposed in this paper indicates that the optimum exploration targets produced, i.e. the eastern and south-eastern portions of the study area, are highly favourable for further exploration of the gold mineralisation. The findings of this study could be summarised as follows:

- incorporation of fractal concepts with outranking approaches, proposed in this paper, achieves better results compared to conventional approaches;
- knowledge deficiency on the understanding of complex mineral systems could be redressed by the use of fractal concepts in terms of classification of exploration evidence data;
- outranking approaches are able to integrate indicator layers derived from multi-disciplinary geospatial data sets, in order to generate reliable exploration targets;
- the conventional TOPSIS method proved to be more efficient than the VIKOR, index overlay, and other variants of the TOPSIS;
- in gold prospectivity mapping, geochemical criterion and Au indicator layer had the highest impact on synthesising indicator layers.

Acknowledgements. The authors would like to express their sincere thanks to the School of Mining Engineering, University of Tehran, for all their support. We also thank to two anonymous referees for their constructive and valuable comments which helped us improve the quality of the work.

REFERENCES

Abedi M.; 2015: *Reply to the comment by B. Ghobadipour and B. Mojarradi "M. Abedi, S.A. Torabi, G.-H. Norouzi and M. Hamzeh; ELECTRE III: a knowledge-driven method for integration of geophysical data with geological and geochemical data in mineral prospectivity mapping*". J. Appl. Geophys., **117**, 138-140.

Abedi M. and Norouzi G.H.; 2012: *Integration of various geophysical data with geological and geochemical data to determine additional drilling for copper exploration*. J. Appl. Geophys., **83**, 35-45.

Abedi M. and Norouzi G.H.; 2016: *A general framework of TOPSIS method for integration of airborne geophysics, satellite imagery, geochemical and geological data*. Int. J. Appl. Earth Obs. Geoinf., **46**, 31-44.

Abedi M. and Oskooi B.; 2015: *A combined magnetometry and gravity study across Zagros orogeny in Iran*. Tectonophys., **664**, 164-175.

Abedi M., Norouzi G.H. and Bahroudi A.; 2012a: *Support vector machine for multi-classification of mineral prospectivity areas*. Comput. Geosci., **46**, 272-283.

Abedi M., Torabi S.A., Norouzi G.H. and Hamzeh M.; 2012b: *ELECTRE III: a knowledge-driven method for integration of geophysical data with geological and geochemical data in mineral prospectivity mapping*. J. Appl. Geophys., **87**, 9-18.

Abedi M., Torabi S.A., Norouzi G.H., Hamzeh M. and Elyasi G.R.; 2012c: *PROMETHEE II: a knowledge-driven method for copper exploration*. Comput. Geosci., **46**, 255-263.

Abedi M., Norouzi G.H. and Fathianpour N.; 2013a: *Fuzzy outranking approach: a knowledge-driven method for mineral prospectivity mapping*. Int. J. Appl. Earth Obs. Geoinf., **21**, 556-567.

Abedi M., Norouzi G.H. and Torabi S.A.; 2013b: *Clustering of mineral prospectivity area as an unsupervised classification approach to explore copper deposit*. Arabian J. Geosci., **6,** 3601-3613.

Abedi M., Torabi S.A. and Norouzi G.H.; 2013c: *Application of fuzzy AHP method to integrate geophysical data in a prospect scale, a case study: Seridune copper deposit*. Boll. Geof. Teor. Appl., **54**, 145-164.

Abedi M., Norouzi G.H. and Fathianpour N.; 2015: *Mineral potential mapping in central Iran using fuzzy ordered weighted averaging method*. Geophys. Prospect., **63**, 461-477.

Abedi M., Mohammadi R., Norouzi G.H. and Mohammadi M.S.M.; 2016: *A comprehensive VIKOR method for integration of various exploratory data in mineral potential mapping*. Arabian J. Geosci., **9**, 1-21.

Abedi M., Mostafavi Kashani S.B., Norouzi G.H. and Yousefi M.; 2017: *A deposit scale mineral prospectivity analysis: a comparison of various knowledge-driven approaches for porphyry copper targeting in Seridune, Iran*. J. Afr. Earth Sci., **128**, 127-146.

Afzal P., Heidari S.M., Ghaderi M. and Yasrebi A.B.; 2017: *Determination of mineralization stages using correlation between geochemical fractal modelling and geological data in Arabshah sedimentary rock-hosted epithermal gold deposit, NW Iran*. Ore Geol. Rev., **91**, 278-295.

Agterberg F.P. and Bonham-Carter G.F.; 1999: *Logistic regression and weights of evidence modelling in mineral exploration*. In: Proc., 28th International Symposium on Applications of Computer in the Mineral Industry (APCOM), Golden, CO, USA, vol. 483, p. 490.

Agterberg F.P., Bonham-Carter G.F. and Wright D.F.; 1990: *Statistical pattern integration for mineral exploration*. Comput. Appl. Resour. Est., 1-21.

Ahmadfaraj M., Mirmohammadi M., Afzal P., Yasrebi A.B. and Carranza E.J.; 2019: *Fractal modelling and fry analysis of the relationship between structures and Cu mineralization in Saveh region, central Iran*. Ore Geol. Rev., **107**, 172-185.

Ahrens L.H.; 1954: *The lognormal distribution of the elements (a fundamental law of geochemistry and its subsidiary)*. Geochim. Cosmochim. Acta, **5**, 49-73.

Aitchison J.; 1986: *The statistical analysis of compositional data*. Chapman and Hall., London, UK, 416 pp.

Alavi M.; 1994: *Tectonics of the Zagros orogenic belt of Iran: new data and interpretations*. Tectonophys., **229**, 211-238.

Aliyari F., Rastad E., Mohajjel M. and Arehart G.B.; 2009: *Geology and geochemistry of D-O-C isotope systematics of the Qolqoleh gold deposit, northwestern Iran: implications for ore genesis*. Ore Geol. Rev., **36**, 306-314.

Aliyari F., Rastad E. and Mohajjel M.; 2012: *Gold deposits in the Sanandaj - Sirjan zone: orogenic gold deposits or intrusion - related gold systems?* Resour. Geol., **62**, 296-315.

Aliyari F., Rastad E., Goldfarb R.J. and Sharif J.A.; 2014: *Geochemistry of hydrothermal alteration at the Qolqoleh gold deposit, northern Sanandaj - Sirjan metamorphic belt, northwestern Iran: vectors to high-grade ore bodies*. J. Geochem. Explor., **140**, 111-125.

Almasi A., Jafarirad A., Kheyrollahi H., Rahimi M. and Afzal P.; 2014: *Evaluation of structural and geological factors in orogenic gold type mineralisation in the Kervian area, north-west Iran, using airborne geophysical data*. Explor. Geophys., **45**, 261-270.

Almasi A., Yousefi M. and Carranza E.J.M.; 2017: *Prospectivity analysis of orogenic gold deposits in Saqez - Sardasht goldfield, Zagros orogen, Iran*. Ore Geol. Rev., **91**, 1066-1080.

Asghari G., Alipour S., Azizi H. and Mirnejad H.; 2018: *Geology and mineral chemistry of gold mineralization in Mirge - Naqshineh occurrence (Saqez, NW Iran): implications for transportation and precipitation of gold*. Acta Geol. Sin., **92**, 210-224.

Bai J., Porwal A., Hart C., Ford A. and Yu L.; 2010: *Mapping geochemical singularity using multifractal analysis: application to anomaly definition on stream sediments data from Fun in Sheet, Yunnan, China*. J. Geochem. Explor., **104**, 1-11.

Bladh K.W.; 1982: *The formation of goethite, jarosite, and alunite during the weathering of sulphide - bearing felsic rocks*. Econ. Geol., **77**, 176-184.

Bonham-Carter G.F.; 1994: *Geographic information systems for geoscientists: modelling with GIS, 1st ed*. Elsevier, Amsterdam, The Netherlands, 416 pp.

Bonham-Carter G.F., Agterberg F.P. and Wright D.F.; 1989: *Weights of evidence modelling: a new approach to mapping mineral potential*. In: Agterberg F.P. and Bonham-Carter G.F. (eds), Statistical Applications in the Earth Sciences, Geological Survey Canada, Paper 89-9, pp. 171-183.

Borovec Z.; 1996: *Evaluation of the concentrations of trace elements in stream sediments by factor and cluster analysis and the sequential extraction procedure*. Sci. Total. Environ., **177**, 237-250.

Bufardi A., Gheorghe R. and Xirouchakis P.; 2008: *Fuzzy outranking methods: recent developments*. In: Kahraman C. (ed), Fuzzy Multi-Criteria Decision Making, Springer Optimization and Its Applications, Springer, Boston, MA, USA, vol. 16, pp. 119-157, doi: 10.1007/978-0-387-76813-7_5.

Carranza E.J.M.; 2009: *Geochemical anomaly and mineral prospectivity mapping in GIS*. Handbook of exploration and environmental geochemistry, Elsevier, Amsterdam, The Netherlands, vol. 11, 359 pp.

Carranza E.J.M. and Hale M.; 2001: *Logistic regression for geologically constrained mapping of gold potential, Baguio district, Philippines*. Explor. Min. Geol., **10**, 165-175.

Carranza E.J.M. and Hale M.; 2002a: *Spatial association of mineral occurrences and curvilinear geological features*. Math. Geol., **34**, 203-221.

Carranza E.J.M. and Hale M.; 2002b*: Where are porphyry copper deposits spatially localized? A case study in Benguet province, Philippines*. Nat. Resour. Res., **11**, 45-59.

Carranza E.J.M. and Hale M.; 2002c: *Wildcat mapping of gold potential, Baguio district, Philippines*. Appl. Earth Sci., **111**, 100-105.

Carranza E.J.M. and Hale M.; 2003: *Evidential belief functions for data-driven geologically constrained mapping of gold potential, Baguio district, Philippines*. Ore Geol. Rev., **22**, 117-132.

Carranza E.J.M. and Sadeghi M.; 2010: *Predictive mapping of prospectivity and quantitative estimation of undiscovered VMS deposits in Skellefte district (Sweden)*. Ore Geol. Rev., **38**, 219-241.

Carranza E.J.M. and Laborte A.G.; 2015a: *Random forest predictive modelling of mineral prospectivity with small number of prospects and data with missing values in Abra (Philippines)*. Comput. Geosci., **74**, 60-70.

Carranza E.J.M. and Laborte A.G.; 2015b: *Data-driven predictive mapping of gold prospectivity, Baguio district, Philippines: application of random forests algorithm*. Ore Geol. Rev., **71**, 777-787.

Carranza E.J.M. and Laborte A.G.; 2016: *Data-driven predictive modelling of mineral prospectivity using random forests: a case study in Catanduanes Island (Philippines)*. Nat. Resour. Res., **25**, 35-50.

Carranza E.J.M., Mangaoang J.C. and Hale M.; 1999: *Application of mineral exploration models and GIS to generate mineral potential maps as input for optimum land-use planning in the Philippines*. Nat. Resour. Res., **8**, 165-173.

Carranza E.J.M., Woldai T. and Chikambwe E.M.; 2005: *Application of data-driven evidential belief functions to prospectivity mapping for aquamarine-bearing pegmatites, Lundazi district, Zambia*. Nat. Resour. Res., **14**, 47-63.

Carranza E.J.M., van Ruitenbeek F.J.A., Hecker C., van der Meijde M. and van der Meer F.D.; 2008a: *Knowledge-guided data-driven evidential belief modelling of mineral prospectivity in Cabo de Gata, SE Spain*. Int. J. Appl. Earth Obs. Geoinf., **10**, 374-387.

Carranza E.J.M., Wibowo H., Barritt S.D. and Sumintadireja P.; 2008b: *Spatial data analysis and integration for regional-scale geothermal potential mapping, west Java, Indonesia*. Geotherm., **37**, 267-299.

Cheng Q.; 1995: *The perimeter-area fractal model and its application to geology*. Math. Geol., **27**, 69-82.

Cheng Q.; 1999: *Spatial and scaling modelling for geochemical anomaly separation*. J. Geochem. Explor., **65**, 175-194.

Cheng Q., Agterberg F.P. and Ballantyne S.B.; 1994: *The separation of geochemical anomalies from background by fractal methods*. J. Geochem. Explor., **51**, 109-130.

Chen S.J. and Hwang C.L.; 1992: *Fuzzy multiple attribute decision making: methods and applications*. Springer-Verlag, Berlin, Germany, 548 pp., doi: 10.1007/978-3-642-46768-4.

Deng H., Yeh C.H. and Willis R.J.; 2000: *Inter-company comparison using modified TOPSIS with objective weights*. Comput. Oper. Res., **27**, 963-973.

Dewey J.W. and Grantz A.; 1973: *The Ghir earthquake of April 10, 1972 in the Zagros Mountains of southern Iran: seismotectonic aspects and some results of a field reconnaissance*. Bull. Seismol. Soc. Am., **63**, 2071-2090.

Eberle D.G. and Paasche H.; 2012: *Integrated data analysis for mineral exploration: a case study of clustering satellite imagery, airborne gamma-ray, and regional geochemical data suites*. Geophys., **77**, B167-B176.

Gupta U.G. and Clarke R.E.; 1996: *Theory and applications of the Delphi technique: a bibliography (1975-1994)*. Technol. Forecast. Soc. Change, **53**, 185-211.

Harris D., Zurcher L., Stanley M., Marlow J. and Pan G.; 2003: *A comparative analysis of favorability mappings by weights of evidence, probabilistic neural networks, discriminant analysis, and logistic regression*. Nat. Resour. Res., **12**, 241-255.

Hassanpour S. and Afzal P.; 2013: *Application of concentration-number (C-N) multifractal modelling for geochemical anomaly separation in Haftcheshmeh porphyry system, NW Iran*. Arabian J. Geosci., **6**, 957-970.

Hauke J. and Kossowski T.; 2011: *Comparison of values of Pearson's and Spearman's correlation coefficients on the same sets of data*. Quaestiones Geographicae, **30**, 87-93.

Hawkes R.A.W. and Webb H.E.; 1979: *Geochemistry in mineral exploration, 2nd ed*. Academic Press, New York, NY, USA, 657 pp.

Hosseini S.A. and Abedi M.; 2015: *Data envelopment analysis: a knowledge-driven method for mineral prospectivity mapping*. Comput. Geosci., **82**, 111-119.

Hosseini S.A., Afzal P., Sadeghi B., Sharmad T., Shahrokhi S.V. and Farhadinejad T.; 2015: *Prospection of Au mineralization based on stream sediments and lithogeochemical data using multifractal modelling in Alut 1:100,000 sheet, NW Iran*. Arabian J. Geosci., **8**, 3867-3879.

Hwang C.L. and Yoon K.; 1981: *Multiple attribute decision making: methods and applications a state-of-the-art survey*. Springer-Verlag, Berlin-Heidelberg, Germany, 280 pp., doi: 10.1007/978-3-642-48318-9.

Jahan A., Mustapha F., Ismail M.Y., Sapuan S.M. and Bahraminasab M.; 2011: *A comprehensive VIKOR method for material selection*. Mater. Des., **32**, 1215-1221.

Knight J.E.; 1977: *A thermochemical study of alunite, enargite, luzonite, and tennantite deposits*. Econ. Geol., **72**, 1321-1336.

Li C., Ma T. and Shi J.; 2003: *Application of a fractal method relating concentrations and distances for separation of geochemical anomalies from background*. J. Geochem. Explor., **77**, 167-175.

Linstone H.A. and Turoff M. (eds); 2002: *The Delphi method: techniques and applications*. Addison-Wesley Publishing Company Inc., Reading, MA, USA, 616 pp.

Mandelbrot B.B.; 1983: *The fractal geometry of nature*. W.H. Freeman and Co., San Francisco, CA, USA, 468 pp.

Mao Z., Peng S., Lai J., Shao Y. and Yang B.; 2004: *Fractal study of geochemical prospecting data in south area of Fenghuanshan copper deposit, Tongling Anhui*. J. Earth Sci. Environ., **26,** 11-14.

Mars J. and Rowan L.C.; 2006: *Regional mapping of phyllic- and argillic-altered rocks in the Zagros magmatic arc, Iran, using Advanced Spaceborne Thermal Emission and Reflection Radiometer (ASTER) data and logical operator algorithms*. Geosphere, **2**, 161-186.

Masoudi F.; 1997: *Contact metamorphism and pegmatite development in the region SW of Arak. Iran*. Unpublished.

McCuaig T.C. and Hronsky J.M.; 2000: *The current status and future of the interface between the exploration industry and economic geology research*. SEG Rev., **13,** 553-559.

McCuaig T.C. and Hronsky J.; 2014: *The mineral system concept: key to predictive exploration targeting*. In: Kelly K.D. and Golden H.C. (eds), Building Exploration Capability for the 21st Century, Society of Economic Geologists, Littleton, CO, USA, vol. 18, pp. 153-175.

Miller H.G. and Singh V.; 1994: *Potential field tilt-a new concept for location of potential field sources*. J. Appl. Geophys., **32**, 213-217.

Mohajjel M., Fergusson C.L. and Sahandi M.R.; 2003: *Cretaceous-Tertiary convergence and continental collision, Sanandaj - Sirjan zone, western Iran*. J. Asian Earth Sci., **21**, 397-412.

Mohammadzadeh M. and Nasseri A.; 2018: *Geochemical modelling of orogenic gold deposit using PCANN hybrid method in the Alut, Kurdistan province, Iran*. J. African Earth Sci., **139**, 173-183.

Mohebi A., Mirnejad H., Lentz D., Behzadi M., Dolati A., Kani A. and Taghizadeh H.; 2015: *Controls on porphyry Cu mineralization around Hanza Mountain, south-east of Iran: an analysis of structural evolution from remote sensing, geophysical, geochemical and geological data*. Ore Geol. Rev., **69**, 187-198.

Moritz R., Ghazban F. and Singer B.S.; 2006: *Eocene Gold Ore formation at Muteh, Sanandaj - Sirjan tectonic zone, western Iran: a result of late-stage extension and exhumation of metamorphic basement rocks within the Zagros orogen*. Econ. Geol., **101**, 1497-1524.

Morrison G.W., Teale G.S. and Hodkinson I.; 1987: *Geology and gold mineralization at Mount Leyshon, North Queensland*. In: Proc., Pacific Rim Congress 87, Gold Coast, Queensland, Australia, pp. 777-780.

Nazarpour A.; 2018: *Application of C-A fractal model and exploratory data analysis (EDA) to delineate geochemical anomalies in the: Takab 1:25,000 geochemical sheet, NW Iran*. Iran. J. Earth Sci., **10**, 173-180.

Nykänen V.; 2008: *Radial basis functional link nets used as a prospectivity mapping tool for orogenic gold deposits within the central Lapland Greenstone belt, northern Fennoscandian shield*. Nat. Resour. Res., **17**, 29-48.

Opricovic S.; 1998: *Multicriteria optimization of civil engineering systems*. Ph. D. Thesis, Faculty of Civil Engineering, Belgrade, 302 pp.

Opricovic S. and Tzeng G.H.; 2004: *Compromise solution by MCDM methods: a comparative analysis of VIKOR and TOPSIS*. Eur. J. Oper. Res., **156**, 445-455.

Oskooi B. and Abedi M.; 2015: *An airborne magnetometry study across Zagros collision zone along Ahvaz–Isfahan route in Iran*. J. Appl. Geophys., **123**, 112-122.

Panahi S., Khakzad A. and Afzal P.; 2017: *Application of Step-wise Weight Assessment Ratio Analysis (SWARA) for copper prospectivity mapping in Anarak region, central Iran*. Arabian J. Geosci., **10**, 484.

Pazand K. and Hezarkhani A.; 2015: *Porphyry Cu potential area selection using the combine AHP - TOPSIS methods: a case study in Siahrud area (NW, Iran)*. Earth Sci. Inf., **8**, 207-220.

Pazand K., Hezarkhani A. and Ataei M.; 2012: *Using TOPSIS approaches for predictive porphyry Cu potential mapping: a case study in Ahar - Arasbaran area (NW, Iran)*. Comput. Geosci., **49**, 62-71.

Poormirzaee R. and Oskouei M.M.; 2010: *Use of spectral analysis for detection of alterations in ETM data, Yazd, Iran*. Appl. Geomatics, **2**, 147-154.

Porwal A., Carranza E.J.M. and Hale M.; 2006: *Bayesian network classifiers for mineral potential mapping*. Comput. Geosci., **32**, 1-16.

Ren L., Zhang Y., Wang Y. and Sun Z.; 2007: *Comparative analysis of a novel MTOPSIS method and TOPSIS*. Appl. Math. Res. Express, vol. 2007, 10 pp., doi:10.1093/amrx/abm005.

Rezaei S., Lotfi M., Afzal P., Jafari M.R. and Shamseddin Meigoony M.; 2015: *Prospecting of copper and gold occurrences using multifractal modelling with index overlay integration in Saveh 1:100,000 sheet, central Iran*. Miner. Resour. Manage., **31**, 51-74.

Richards J.P., Wilkinson D. and Ullrich T.; 2006: *Geology of the Sari Gunay epithermal gold deposit, northwest Iran*. Econ. Geol., **101**, 1455-1496.

Roy B.; 1974: *Critères multiples et modélisation des préférences (l'apport des relations de surclassement)*. Rev. Econ. Polit., **84**, 1-44.

Scott K.M.; 1990: *Origin of alunite- and jarosite-group minerals in the Mt. Leyshon epithermal gold deposit, northeast Queensland, Australia*. Am. Mineral., **75**, 1176-1181.

Shahsavar S., Jafari Rad A., Afzal P., Nezafati N. and Akhavan Aghdam M.; 2019: *Prospecting for polymetallic mineralization using step-wise weight assessment ratio analysis (SWARA) and fractal modelling in Aghkand area, NW Iran*. Arabian J. Geosci., **12**, 248-257.

Skulmoski G.J., Hartman F.T. and Krahn J.; 2007: *The Delphi method for graduate research*. J. Inf. Technol. Educ., **6**, 1-21.

Tavana M. and Hatami-Marbini A.; 2011: *A group AHP-TOPSIS framework for human spaceflight mission planning at NASA*. Expert Syst. Appl., **38**, 13588-13603.

van Helvoort P.-J., Filzmoser P. and van Gaans P.F.M.; 2005: *Sequential factor analysis as a new approach to multivariate analysis of heterogeneous geochemical data sets: an application to a bulk chemical characterization of fluvial deposits (Rhine - Meuse delta, The Netherlands)*. Appl. Geochem., **20**, 2233-2251.

Yarmohammadi A.; 2006: *Mineralogy, geochemistry, structure, texture and genesis of gold (Ag, base metals and barite) in Barika mineral area (east of Sardasht), Iran*. MS thesis, Tarbiat Modares University, Iran.

Yousefi M. and Carranza E.J.M.; 2015a: *Fuzzification of continuous-value spatial evidence for mineral prospectivity mapping*. Comput. Geosci., **74**, 97-109.

Yousefi M. and Carranza E.J.M.; 2015b: *Prediction-area (P-A) plot and C-A fractal analysis to classify and evaluate evidential maps for mineral prospectivity modelling*. Comput. Geosci., **79**, 69-81.

Yousefi M. and Carranza E.J.M.; 2015c: *Geometric average of spatial evidence data layers: a GIS-based multi-criteria decision-making approach to mineral prospectivity mapping*. Comput. Geosci., **83**, 72-79.

Yousefi M. and Carranza E.J.M.; 2016: *Data-driven index overlay and boolean logic mineral prospectivity modelling in greenfields exploration*. Nat. Resour. Res., **25**, 3-18.

Yousefi M. and Carranza E.J.M.; 2017: *Union score and fuzzy logic mineral prospectivity mapping using discretized and continuous spatial evidence values*. J. Afr. Earth Sci., **128**, 47-60.

Yousefi M. and Nykänen V.; 2017: *Introduction to the special issue: GIS-based mineral potential targeting*. J. Afr. Earth Sci., **128**, 1-4.

Yousefi M., Kamkar-Rouhani A. and Carranza E.J.M.; 2014: *Application of staged factor analysis and logistic function to create a fuzzy stream sediment geochemical evidence layer for mineral prospectivity mapping*. Geochem. Explor. Environ. Anal., **14**, 45-58.

Zadmehr F. and Shahrokhi S.V.; 2019: *Separation of geochemical anomalies by concentration-area and concentration-number methods in the Saqez 1:100,000 Sheet, Kurdistan*. Iran. J. Earth Sci., **11,** 196-204.

Zuo R. and Carranza E.J.M.; 2011: *Support vector machine: a tool for mapping mineral prospectivity*. Comput. Geosci., **37**, 1967-1975.

Corresponding author: Maysam Abedi
School of Mining Engineering, College of Engineering, University of Tehran
North Kargar Street, Tehran, Iran
Phone: +98 0216 1114563, e-mail: MaysamAbedi@ut.ac.ir

Appendix A1: The VIKOR method

The VIKOR method was introduced by Opricovic (1998) as a powerful technique in the MCDM problems to rank diverse attributes under different criteria, where it ranks and selects from a set of alternatives in the presence of conflicting multi-criteria. It introduces the multi-criteria ranking index based upon the measure of "closeness" to the "ideal solution" (Opricovic, 1998; Opricovic and Tzeng, 2004). The formulation of the conventional C-VIKOR and the adjusted A-VIKOR versions are as follows.

Let us assume that $A_i (i = 1, 2, ..., n)$ and $C_j (j = 1, 2, ..., m)$ are a set of n alternatives and m criteria/attributes respectively. The C-VIKOR method can be described in a series of steps.

Step 1: construct a decision matrix acquired from the geoscience data sets by assigning a priority score: $X = (x_{ij})_{n\times m}$ to each alternative i on each criterion j.

Step 2: determine the important weight (w_j) of all criteria from developed methods (e.g. Delphi in this study) such that:

$$\sum_{j=1}^{m} w_j = 1, \quad j = 1, 2, \ldots, \ m . \tag{A-1}$$

Step 3: obtain the normalised decision matrix (r_{ij}) to avoid scaling effects perturbing the MPM result:

$$r_{ij} = x_{ij} / \left(\sum_{p=1}^{n} x_{pj}^2 \right)^{0.5}, \quad i = 1, 2, \ldots, \ n \quad j = 1, 2, \ldots, \ m . \tag{A-2}$$

Step 4: determine the best f_j^+ and the worst f_j^- values of all criteria:

$$f_j^+ = \left(f_1^+, f_2^+, \ \ldots, \ f_j^+, \ \ldots, f_m^+ \right) = \left\{ \left(\max_i \left\{ r_{ij} \right\} \middle| j \in B \right), \left(\min_i \left\{ r_{ij} \right\} \middle| j \in C \right) \right\} \tag{A-3}$$

$$f_j^- = \left(f_1^-, f_2^-, \ \ldots, \ f_j^-, \ \ldots, \ f_m^- \right) = \left\{ \left(\min_i \left\{ r_{ij} \right\} \middle| j \in B \right), \left(\max_i \left\{ r_{ij} \right\} \middle| j \in C \right) \right\} \tag{A-4}$$

where B and C correspond to the benefit and cost criteria, respectively (Tavana and Hatami-Marbini, 2011).

Step 5: compute the values of S_i and R_i from the following equation. Development of the VIKOR method started from L_k -metric as (Opricovic and Tzeng, 2004):

$$L_{k,i} = \{ \sum_{j=1}^{m} \left[w_j \left(f_j^+ - r_{ij} \right) / \left(f_j^+ - f_j^- \right) \right]^k \}^{1/k} , \quad 1 \le k \le \infty. \tag{A-5}$$

Here the values of S_i and R_i are calculated from Eq. A-5:

$$S_i = L_{1,i} = \sum_{j=1}^{m} w_j \left(f_j^+ - r_{ij} \right) / \left(f_j^+ - f_j^- \right) \tag{A-6}$$

$$R_i = L_{\infty,i} = \max_j \left(w_j \left(f_j^+ - r_{ij} \right) / \left(f_j^+ - f_j^- \right) \right) . \tag{A-7}$$

Step 6: compute the values of Q_i for each alternative i from the following equation:

$$Q_i = v \left(\frac{S_i - S^-}{S^+ - S^-} \right) + (1 - v) \left(\frac{R_i - R^-}{R^+ - R^-} \right), \quad 0 \le v \le 1 \tag{A-8}$$

where:

$$\begin{cases} S^+ = \max_i S_i, \; S^- = \min_i S_i \\ R^+ = \max_i R_i, \; R^- = \min_i R_i \end{cases}$$

and parameter v is introduced as a weight for the strategy of the majority of criteria "$\frac{S_i - S^-}{S^+ - S^-}$" and $(1 - v)$ is the weight of the individual regret "$\frac{R_i - R^-}{R^+ - R^-}$". The value of v lies in a range of [0, 1] and in most cases it was chosen equal to $v = 0.5$ for a compromise solution (Abedi *et al*., 2016).

Step 7: compute MPM values of M_i for final prospectivity mapping as:

$$M_i^{V-C} = \frac{Q^+ - Q_i}{Q^+ - Q^-} \tag{A-9}$$

where: $Q^+ = \max_i Q_i$ and $Q^- = \min_i Q_i$. Higher values of M_i^{V-C} correspond to higher potential zones for ore occurrences in the region of interest.

To implement the A-VIKOR proposed by Jahan *et al*. (2011), the values of S_i and R_i are calculated from the following equations while the other steps are similar to the C-VIKOR method for the calculation of M_i^{V-A}:

$$S_i = \sum_{j=1}^{m} w_j \left(1 - e^{\frac{\left| r_{ij} - f_j^+ \right|}{f_j^- - f_j^+}} \right) \tag{A-10}$$

$$R_i = \max_j \left[w_j \left(1 - e^{\frac{\left| r_{ij} - f_j^+ \right|}{f_j^- - f_j^+}} \right) \right]. \quad \text{(A-11)}$$

Appendix A2: The TOPSIS method

The TOPSIS method was first presented by Hwang and Yoon (1981) and later developed by Chen and Hwang (1992). Its basic principle is that the chosen alternative should have the shortest distance from the positive ideal solution (PIS) and the farthest distance from the negative ideal solution (NIS) (Opricovic and Tzeng, 2004; Tavana and Hatami-Marbini, 2011; Pazand *et al*., 2012; Pazand and Hezarkhani, 2015). Here, the precise and concise procedure of three prevalent variants of the TOPSIS method: 1) the conventional TOPSIS or C-TOPSIS (Hwang and Yoon, 1981), 2) the adjusted TOPSIS or A-TOPSIS (Deng *et al*., 2000), and 3) the modified TOPSIS or M-TOPSIS (Ren *et al*., 2007) are described.

The formulation of the conventional method can be described in a series of steps.

Steps 1-3: similar to the steps of the C-VIKOR method.

Step 4: obtain the weighted normalised decision matrix of V_{ij}:

$$V_{ij} = w_j r_{ij}, \quad i = 1, 2, \ldots, n \text{ and } j = 1, 2, \ldots, m . \quad \text{(A-12)}$$

Step 5: determine the PIS and NIS values, respectively, as:

$$f_j^+ = \left(v_1^+, v_2^+, \ldots, v_j^+, \ldots, v_m^+ \right) = \left\{ \left(\max_i \left\{ v_{ij} \right\} \middle| j \in B \right), \left(\min_i \left\{ v_{ij} \right\} \middle| j \in C \right) \right\} \quad \text{(A-13)}$$

$$f_j^- = \left(v_1^-, v_2^-, \ldots, v_j^-, \ldots, v_m^- \right) = \left\{ \left(\min_i \left\{ v_{ij} \right\} \middle| j \in B \right), \left(\max_i \left\{ v_{ij} \right\} \middle| j \in C \right) \right\}. \quad \text{(A-14)}$$

Step 6: compute the separation measures $M = (S_i^+, S_i^-)$ by the Euclidean distance as follows:

$$S_i^+ = \left\{ \sum_{j=1}^{m} \left(v_{ij} - v_j^+ \right)^2 \right\}^{0.5}; \quad i = 1, \ldots, n \quad \text{(A-15)}$$

$$S_i^- = \left\{ \sum_{j=1}^{m} \left(v_{ij} - v_j^- \right)^2 \right\}^{0.5}; \quad i = 1, \ldots, n . \quad \text{(A-16)}$$

Step 7: calculate the relative closeness of the alternatives to the ideal solution as follows:

$$T_i^C = \frac{S_i^-}{S_i^+ + S_i^-}; \quad i = 1, \ldots, n . \quad \text{(A-17)}$$

Step 8: compute the normalised MPM values of M_i^{T-C} for the final prospectivity mapping as:

$$M_i^{T-C} = \frac{T_i^C - \min_i\left(T_i^C\right)}{\max_i\left(T_i^C\right) - \min_i\left(T_i^C\right)}; \quad i = 1, \ldots, n \quad 0 \le M_i^C \le 1 \tag{A-18}$$

where high and low values of M_i^{T-C} correspond to the high and low potential zones, respectively (Abedi and Norouzi, 2016).

The extended version of the C-TOPSIS method was presented by Deng *et al*. (2000), whereby the weighted Euclidian distances are incorporated in the conventional algorithm rather than creating a weighted decision matrix of V_{ij}. The A-TOPSIS method consists of the following steps.

Steps 1-3: similar to the steps of the C-VIKOR method.

Step 4: determine the PIS and NIS values, respectively, as:

$$f_j^+ = \left(v_1^+, v_2^+, \ldots, v_j^+, \ldots, v_m^+\right) = \left\{ \left(\max_i\left\{r_{ij}\right\} \middle| j \in B\right), \left(\min_i\left\{r_{ij}\right\} \middle| j \in C\right) \right\} \tag{A-19}$$

$$f_j^- = \left(v_1^-, v_2^-, \ldots, v_j^-, \ldots, v_m^-\right) = \left\{ \left(\min_i\left\{r_{ij}\right\} \middle| j \in B\right), \left(\max_i\left\{r_{ij}\right\} \middle| j \in C\right) \right\}. \tag{A-20}$$

Step 5: compute the weighted Euclidian distances:

$$S_i^+ = \left\{ \sum_{j=1}^{m} w_j\left(r_{ij} - v_j^+\right)^2 \right\}^{0.5}; \quad i = 1, \ldots, n \tag{A-21}$$

$$S_i^- = \left\{ \sum_{j=1}^{m} w_j\left(r_{ij} - v_j^-\right)^2 \right\}^{0.5}; \quad i = 1, \ldots, n. \tag{A-22}$$

Step 6: calculate the relative closeness of the alternatives to the ideal solution as follows:

$$T_i^A = \frac{S_i^-}{S_i^+ + S_i^-}; \quad i = 1, \ldots, n. \tag{A-23}$$

Step 7: compute the normalised MPM values of M_i^{T-A} for the final prospectivity mapping as (Abedi and Norouzi, 2016):

$$M_i^{T-A} = \frac{T_i^A - \min_i\left(T_i^A\right)}{\max_i\left(T_i^A\right) - \min_i\left(T_i^A\right)}; \quad i = 1, \ldots, n \quad 0 \le M_i^A \le 1. \tag{A-24}$$

Ren *et al*. (2007) introduced the M-TOPSIS method based upon the concept of the original TOPSIS to avoid rank reversal of alternatives and to solve the problem on evaluation failure that often occurs in the C-TOPSIS method. The formulation of this method can be described in a series of steps as follows.

Steps 1-5: similar to the steps of the C-TOPSIS method.

Step 6: determine the ideal reference point *S*:

$$S = \left(S^I,\ S^N\right) = \left(min\left(S_i^+\right), max\left(S_i^-\right)\right);\quad i = 1,\ \ldots,\ n. \tag{A-25}$$

Step 7: calculate the Euclidian distance between the point S and the values of S_i^+ and S_i^- for each alternative as follows:

$$T_i^M = \left\{\left(S_i^+ - S^I\right)^2 + \left(S_i^- - S^N\right)^2\right\}^{0.5};\quad i = 1,\ \ldots,\ n. \tag{A-26}$$

Step 8: compute the normalised MPM values of M_i^{T-M} for the final prospectivity mapping as (Abedi and Norouzi, 2016):

$$M_i^{T-M} = \frac{\max\limits_i\left(T_i^M\right) - T_i^M}{\max\limits_i\left(T_i^M\right) - \min\limits_i\left(T_i^M\right)};\quad i = 1, \ldots,\ n \quad 0 \le M_i^M \le 1. \tag{A-27}$$

Appendix A3: Concentration-number fractal model

Separation of anomalous regions from the background is an important aim in geochemical exploration studies, where various conventional approaches on the basis of classical statistics have been utilised to identify the threshold values for separating different geochemical populations within a sought region (Hawkes and Webb, 1979; Li *et al*., 2003). It is worth mentioning that a threshold value equal to the sum of mean and 1.5 to 3.0 times of the standard deviation has been assumed in cases of a normal distribution of an element, but the distribution of many elements does not obey a normal pattern (Ahrens, 1954; Li *et al*., 2003). Another point worth taking into account concerns the spatial distribution of geochemical data as an important key for the separation of geochemical populations, while it is not considered in conventional statistical methods. In addition, they have less capability in identifying the weak anomalous regions when located in a high value of background (Bai *et al*., 2010). To tackle such weakness in geochemical data processing, fractal theory as an important non-Euclidean method in geometry was introduced (Mandelbrot, 1983). Various researchers have focused on developing several variants of fractal geometry in geosciences applications. Cheng *et al*. (1994) and Cheng (1995) proposed concentration-area (C-A) and concentration-perimeter (C-P) methods for the separation of geochemical anomalies from the background accompanied with a calculation of elemental thresholds. Other fractal methods have been used, such as power spectrum-area (S-A) by Cheng (1999), concentration-distance (C–D) by Li *et al*. (2003), and concentration-number (C-N) by Mao *et al*. (2004). In this study, the C-N fractal method was applied for the geochemical population separation. Mao *et al*. (2004) proposed the C-N method as a branch of C-A model. The model has a general form of:

$$N(\geq\rho) \propto \rho^{-\beta} \tag{A-28}$$

where $N(\geq\varrho)$ denotes the sample number with concentration values higher than the ϱ value, and β is the fractal dimension. The main advantage of this fractal variant is no pre-treatment and evaluation of the geochemical data.

Appendix A4: Spearman correlation coefficient

This is a non-parametric measure of rank correlation which determines statistical dependence between the rankings of two variables. This coefficient is similar to the Pearson correlation between the rank values of the two variables. Note that Pearson's correlation coefficient assesses a linear relationship while Spearman's correlation assumes a monotonic relationship (whether linear or not). When the variables are not normally distributed or the relationship between the variables is non-linear, we use the Spearman rank correlation method (Hauke and Kossowski, 2011).